Planetary and Space Science 85 (2013) 106–122

Contents lists available at ScienceDirect

Planetary and Space Science

journal homepage: www.elsevier.com/locate/pss

Phobos interior from librations determination using Doppler and star tracker measurements

Sebastien Le Maistre[a,*], Pascal Rosenblatt[a], Nicolas Rambaux[b], Julie C. Castillo-Rogez[c], Veronique Dehant[a], Jean-Charles Marty[d]

[a] Royal Observatory of Belgium, av. Circulaire 3, Brussels 1180, Belgium
[b] IMCCE, Observatoire de Paris, av. denfert-Rochereau 77, Paris 75014, France
[c] Jet Propulsion Laboratory, California Institute of Technology, Pasadena, CA, USA
[d] Centre National d'Etudes Spatiales, av. Edouard Belin 18, Toulouse 31401, France

ARTICLE INFO

Article history:
Received 14 August 2012
Received in revised form
22 May 2013
Accepted 7 June 2013
Available online 25 June 2013

Keywords:
Rotation
Lander
Interior
Libration
Phobos
Doppler
Star tracker
Tidal deformation

ABSTRACT

Numerical simulations have been performed to assess the precision that can be obtained on Phobos libration angles by using two types of data acquired by a probe landed on the Martian moon: (1) Direct-To-Earth (DTE) Doppler data and (2) Star-Tracker (ST) data. Compared to independent estimates, combination of DTE and ST data provides the more precise estimates of Phobos libration angles at the 10^{-3}–10^{-5} degree level. Short period libration amplitudes are functions of the relative moments of inertia. Thus their determination would provide constraints on mass distributions inside Phobos. We show that the longitudinal libration amplitude at the orbital period, while being clearly distinct from the resonance period, is the most interesting signal for that purpose, because it leads to the best precision on $(B-A)/C$ (10^{-5} after only 10 weeks of operation). Nevertheless, we showed that inferring the individual moments of inertia A, B and C with a precision sufficient ($<1\%$) to distinguish the rotational behavior of an homogenous from that of an heterogenous body requires the determination of one of the degree-two gravity field coefficient at the percent level.

In addition, we stress that ST and DTE data combination allows de-correlating librational motion from orbital motion since ST measurements are sensitive to the moon's rotation and do not depend on its ephemeris, whereas DTE Doppler data are sensitive to both motions as well as to Phobos' surface displacement due to the tides raised by Mars. Furthermore, the ephemeris of Phobos has to be known at the centimeter level to allow measuring the tidal surface displacement with enough precision to conclude on the nature of Phobos' interior (rubble pile versus monolithic) as one step toward constraining its origin and evolution.

1. Introduction

Recent technological developments for close proximity and in situ operations are opening the door to a new generation of lander-based missions. Owing to its singular place in the Martian system, Phobos is a favored target for these missions in the frame of prospective human exploration and for better constraining the origin of the Martian system. For the past decade, several mission concepts for the in situ exploration[1] of Phobos have been proposed: *Mars Moon Sample Return* mission (Michel et al., 2011) or *Gravity, Einstein's Theory, and Exploration of the Martian Moons' Environment* also known as GETEMME (Oberst et al., 2012) on the European side and *Hall* (Lee et al., 2010), *Phobos Laser Ranging* or PLR (Turyshev et al., 2010), *Phobos Reconnaissance and International Mars Exploration* or PRIME (Lee et al., 2008), and *Mars Moons Multiple-landings Mission* (Lee et al., 2011) on the US side. Also, a Russian mission named *Phobos-Soil* (Korablev, 2009) was launched in November 2011 but failed shortly after launch, falling down into the Pacific ocean in January 2012.

Phobos is in synchronous spin-orbit resonance around Mars, showing on average the same hemisphere to Mars. This uniform rotational motion is superimposed by oscillations, called physical librations, that result from the time-varying gravitational torque exerted by Mars on the dynamical figure of Phobos. In 2010, by analyzing Phobos images obtained by the SRC (Super Resolution Channel) of the HRSC (High Resolution Stereo Camera) on the European *Mars Express* (MEX) spacecraft, Willner et al. (2010) observed a libration in longitude of amplitude $1.2 \pm 0.15°$. This physical libration of about 500 m peak-to-peak at the surface is one of the largest among all known synchronously orbiting, natural satellites of the solar system. The amplitudes of libration are linked to the mass repartition inside the body and so are an elegant way to obtain information on the interior. Taking as a

* Corresponding author. Tel.: +32 23736755.
E-mail address: sebastien.lemaistre@oma.be (S. Le Maistre).

[1] By "in situ" we refer to landed missions.

0032-0633/$ - see front matter © 2013 Elsevier Ltd. All rights reserved.
http://dx.doi.org/10.1016/j.pss.2013.06.015

reference the payload onboard *Phobos-Soil*, including a star tracker and an X-band coherent transponder, we assess the precision that could be achieved on the determination of Phobos' libration amplitudes using both Direct-To-Earth (DTE) Doppler (as done in Le Maistre et al., 2012 for Mars) and Star Tracker (ST) measurements.

In addition, the tidal deformation of Phobos is evaluated and compared against the estimated precision that could be obtained on the surface displacement by using DTE Doppler data. Phobos' ability to deform depends on its bulk interior, rigidity and composition. Knowing these properties would provide crucial information on its origin and evolution (Rosenblatt, 2011).

To reach these objectives, we perform numerical simulations based on a least-squares techniques. Results from that study stress the value of geodetic measurements for constraining Phobos' interior.

The paper is divided in 13 parts. The model of rotation of Phobos used in this study is presented first in Section 2. Then we describe the data simulation method in Section 3. The precisions that can be achieved on the determination of the libration of Phobos are shown in Section 4 and the lander coordinates estimates, determined using DTE Doppler data simultaneously with rotational parameters, are presented in Section 5. The Phobos ephemeris issue is discussed in Section 6 and the rotation mis-modeling impact on libration amplitude estimates is pointed out in Section 7. We assess then the constraints that can be obtained on the proper frequency (Section 8) and moments of inertia (Section 9) of the Martian moon from the determination of its librations. We shortly discuss in Section 10 about what can be learned on Phobos gravity field and Mars oblateness from a precise measurement of the librations. Finally, we characterize in Section 11 the tides raised by Mars on Phobos' surface as a function of its interior structure and composition and we compare the theoretical radial motion of the lander with the precisions that can be obtained on the tidal displacement determination using radio science measurements. A brief discussion on Phobos dissipation is carried out in Section 12 and key results are summarized in Section 13.

2. Phobos rotational model

In the simulations presented in this paper, we use the most recent model of rotation of Phobos from Rambaux et al. (2012). This model expresses the transformation between Mars' mean equatorial plane at the date and the reference frame tied to Phobos. In the present paper dealing with the observation of Phobos from the Earth, we use the Earth mean equator of J2000 epoch (i.e., the 1st January 2000 at 12 h) as reference frame. Thus, the librational angles expressed in Mars' mean equatorial plane at the date are expressed in the Earth mean equator of J2000 (inertial frame denoted hereafter as EME2000) and the rotation is described through three angles (α, δ, W). The right ascension, α, and the declination, δ, specify the direction of the figure axis of the body. The angle W describes the location of the prime meridian of the body in its equatorial plane. We express these angles as

$$\alpha = \alpha_0 + \dot{\alpha} t + \sum_{T_\alpha} \left(\alpha^c_{T_\alpha} \cos\left(\frac{2\pi}{T_\alpha} t\right) + \alpha^s_{T_\alpha} \sin\left(\frac{2\pi}{T_\alpha} t\right) \right), \tag{1}$$

$$\delta = \delta_0 + \dot{\delta} t + \sum_{T_\delta} \left(\delta^c_{T_\delta} \cos\left(\frac{2\pi}{T_\delta} t\right) + \delta^s_{T_\delta} \sin\left(\frac{2\pi}{T_\delta} t\right) \right), \tag{2}$$

$$W = W_0 + \dot{W} t + \ddot{W} t^2 + \sum_{T_W} \left(W^c_{T_W} \cos\left(\frac{2\pi}{T_W} t\right) + W^s_{T_W} \sin\left(\frac{2\pi}{T_W} t\right) \right) - \Delta\alpha \sin\delta. \tag{3}$$

Table 1
Direction of the North pole of rotation and the prime meridian of Phobos at J2000 derived from the Rambaux et al. (2012) rotational model. Linear and quadratic terms are from Seidelmann et al. (2002).

At J2000	Linear terms	Quadratic terms
$\alpha_0 = 317.65171°$	$\dot{\alpha} = -0.108°$/century	–
$\delta_0 = 52.875277°$	$\dot{\delta} = -0.061°$/century	–
$W_0 = 34.78084°$	$\dot{W} = 1128.844585°$/day	$\ddot{W} = 8.864°/\text{century}^2$

Table 2
Periodic variations of the rotation axis direction and prime meridian of Phobos' figure expressed in amplitudes of sine and cosine derived from the Rambaux et al. (2012) rotational model. The series are truncated at 10^{-4} degree, hence considering only variations greater than 2 cm at the surface of Phobos.

Period (**day**) T_α	**Cosine amplitude** (**deg.**) $\alpha^c_{T_\alpha}$	**Sine amplitude** (**deg.**) $\alpha^s_{T_\alpha}$
Libration in α		
826.2093	0.325245	1.758464
686.9689	3.7879×10^{-3}	-9.9870×10^{-3}
413.1034	8.0360×10^{-3}	2.0727×10^{-2}
0.8430	-5.0099×10^{-3}	1.5865×10^{-2}
0.5133	-1.3858×10^{-2}	-2.6599×10^{-2}
0.2313	-3.0986×10^{-2}	-3.4267×10^{-2}
T_δ	$\delta^c_{T_\delta}$	$\delta^s_{T_\delta}$
Librations in δ		
826.2098	1.059273	−0.200688
686.9603	-5.8509×10^{-3}	-3.1664×10^{-3}
413.0996	6.2752×10^{-3}	-2.3877×10^{-3}
0.8430	9.5540×10^{-3}	3.2837×10^{-3}
0.5133	1.6049×10^{-2}	-8.3571×10^{-3}
0.2313	2.0673×10^{-2}	-1.8695×10^{-2}
T_W	$W^c_{T_W}$	$W^s_{T_W}$
Librations in W		
826.2082	−0.260555	−1.403236
413.1050	-8.1901×10^{-3}	-2.1305×10^{-2}
0.8430	3.9954×10^{-3}	-1.2650×10^{-2}
0.5133	1.1051×10^{-2}	2.1210×10^{-2}
0.3190	0.177178	1.085406
0.2313	2.4709×10^{-2}	2.7324×10^{-2}
0.1595	-2.7638×10^{-3}	-8.2309×10^{-3}

where the sine (cosine) amplitudes are labeled with a superscript "s" ("c"). T_α, T_δ and T_W are the periods of the librational signals. The values of the coefficients are listed in Tables 1 and 2.

These angles are expressed as functions of constant, linear, quadratic, and periodic terms. The α_0, δ_0 represent the position of the rotation axis at J2000, and W_0 describes the location of the prime meridian at J2000. The linear term in W represents the uniform rotational motion of Phobos and the quadratic term is related to the secular acceleration of the orbital motion that is transferred to the rotation through the spin-orbit resonance (Rambaux et al., 2012). The linear term in α and δ and the periodic terms represent the precessional motion of the polar axis of Phobos and its librational motion, respectively.

We introduce the last term in Eq. (3) for the reduction process. In this equation $\Delta\alpha$ is the deviation of the α−libration from its a priori value, i.e., the correction in the orientation of the equatorial plane of Phobos and differs from zero only when $\alpha^c_{T_\alpha}$ and $\alpha^s_{T_\alpha}$ are estimated.

All the periodic terms are called hereafter "Phobos rotation and Orientation Parameters" (POP) or "libration parameters". In the following, the longitudinal librations refer to the W series and latitudinal librations refer to the series in α and δ. Their coefficients and periods are listed in Table 2. The amplitudes reported in that table are those greater than 10^{-4} degree, i.e., the level of detection of the librations through a *Phobos-soil* like experiment (see Section 4). In addition, Table 2 shows that the librations period can be classified in two classes: (1) long period, related to the motion of the nodes of the orbit, that is larger than hundred days and (2) short period, related to the orbital period of the satellite, that is below one day (Chapront-Touzé, 1990; Borderies and Yoder, 1990; Rambaux et al., 2012).

As the polar motion of Phobos is negligible, we do not account for that signal in the rotation model used in this study. Thus, the rotation matrix M that transforms a lander position $\vec{r}_{in}$ from the Phobos mean equator of J2000 (inertial reference frame denoted below PME2000) into a Phobos body-fixed vector $\vec{r}_{bf}$ (i.e., $\vec{r}_{bf} = M\,\vec{r}_{in}$) can be written as follows:

$$M = \underbrace{R_z(W)R_x\left(\frac{\pi}{2}-\delta\right)R_z\left(\frac{\pi}{2}+\alpha\right)}_{M_\Gamma}\underbrace{R_z\left(-\frac{\pi}{2}-\alpha_0\right)R_x\left(-\frac{\pi}{2}+\delta_0\right)}_{M_0}, \tag{4}$$

$$M_\Gamma = \begin{pmatrix} -\cos W\sin\alpha - \cos\alpha\sin\delta\sin W & \sin\alpha\sin\delta\sin W - \cos\alpha\cos W & \cos\delta\sin W \\ \cos\alpha\cos W\sin\delta - \sin\alpha\sin W & -\cos W\sin\alpha\sin\delta - \cos\alpha\sin W & -\cos\delta\cos W \\ \cos\alpha\cos\delta & -\cos\delta\sin\alpha & \sin\delta \end{pmatrix}. \tag{8}$$

with a constant matrix M_0 that rotates $\vec{r}_{in}$ to the position vector $\vec{r}_{icrf}$ expressed in the Earth mean equator of J2000 reference frame (denoted hereafter EME2000) and a time dependent matrix, M_Γ that projects $\vec{r}_{icrf}$ to the rotating frame tied to the moon's surface and named below PBF for Phobos Body-Fixed frame.

3. Data simulation

In order to determine the libration angles of Phobos, two types of measurements can be used: star tracker measurements and Direct-To-Earth Doppler measurements. In this paper we do simulations based on the analysis of such types of data. To generate the simulated datasets, we choose the landing site that was selected for the *Phobos-Soil* mission as it was in the far side (also opposite to the largest crater on Phobos: Stickney) near the equator (see Appendix A). *Phobos-Soil*' landing site was planned to be between 7°N and 21°N of latitude and 214°W to 233°W of longitude (Korablev, 2009). In our study we thus place the lander at a latitude $\varphi = 14°$N and longitude $\lambda = 224°$W.

3.1. Star tracker data

The star tracker instrument measures the attitude of the spacecraft. ST data are quaternions that give the line of sight direction of the star tracker camera with respect to a given reference frame. These attitude quaternions are obtained by comparing the pattern of stars in the field of view of the camera and an onboard star catalog. The viewing field of the ST is typically a cone of a few tens of degrees of aperture (40° for *Phobos-Soil*). Since Phobos has no atmosphere, there is no diffusion of light. Thus the stars can be seen by the ST camera when the Sun is not in its field of view (avoiding Sun glare). In conclusion, the ST data acquisition can be repeated every 0.319 day (Phobos orbital period) and can last a maximum of 24 500 consecutive seconds (just less than 90% of the time).

As attitude quaternions correspond to a rotation matrix, the ST measurements can be considered as a rotation matrix noted M_{ST}. As the lander will be fixed with respect to the ground, the star tracker will provide the rotation matrix M of Phobos

$$M_{ST} = R_\kappa M R_\Phi = R_\kappa M_\Gamma M_0 R_\Phi, \tag{5}$$

where R_κ is the constant but unknown rotation matrix that changes vector's coordinates from PBF to the reference frame of the ST camera, and R_Φ is the constant rotation matrix that transforms a vector expressed in the inertial star catalog reference frame into an inertial vector expressed in the PME2000 frame. By considering that α_0 and δ_0 are well known, $M_0 R_\Phi$ is then a constant and well known rotation matrix. We can thus assume that ST measurements can always be reduced to the following matrix:

$$M^\star_{ST} = M_{ST} R_\Phi^{-1} M_0^{-1} = R_\kappa M_\Gamma. \tag{6}$$

In this paper, we consider an idealistic case where R_κ would be known (see Appendix B for consequences of such a modeling strategy) from a separate experiment (e.g., from imagery). In such a situation, we could easily infer α, δ and W from $M^\star_{ST}$ by calculating

$$M_\Gamma = R_\kappa^{-1} M^\star_{ST}, \tag{7}$$

When none of the three angles is equal to $\pi/2$, an univocal solution can be obtained by computing

$$\alpha = \arctan\left(-\frac{M_\Gamma(3,2)}{M_\Gamma(3,1)}\right), \tag{9}$$

$$\delta = \arcsin\left(+M_\Gamma(3,3)\right), \tag{10}$$

$$W = \arctan\left(-\frac{M_\Gamma(1,3)}{M_\Gamma(2,3)}\right). \tag{11}$$

Under such a hypothesis about the knowledge of R_κ, the ST data provide direct measurements of Phobos rotation and orientation angles that can be considered as three distinct observables: α, δ and W. White noise of 60 arc second is added to such simulated ST data (see Appendix C for impact of data noise level). This noise level corresponds to the *Phobos-Soil* star tracker camera angular resolution[2] and may neglect some effects such as measurement time-tags and thermal drift in sensor and electronics.

3.2. DTE Doppler data

We focus on coherent two-way Doppler measurements in X-band between the lander and one of the Earth Ground Stations (GS). These data, corresponding to a round-trip radio signal, are sensitive to the motion in space of the body on which the probe has landed as shown in detail by Le Maistre et al. (2012) for Mars. The numerical simulations shown in this paper are performed using the GINS (Geodésie par Intégrations Numériques Simultanées) software developed by CNES (Centre National d'Etudes Spatiales) and further adapted for planetary geodesy applications at the Royal Observatory of Belgium. The Doppler observable is modeled using the formulation of Moyer (2000) and is thus obtained by calculating the range rate over a counting time interval. The Doppler noise level is taken to be equal to 0.05 mm/s at 60 s of integration time, which is typical for an X-band two-way Doppler between Mars and Earth. We note that, in the frame of this study, one-way and two-way data only differ by the data noise level (one-way is about five times noisier than two-way with an

[2] From the instrument sheet of the *Libration Celestial Mechanics Experiment* provided in the Announcement of Opportunity for guest investigators for the Russian *Phobos-Soil* mission released by ESA and Roscosmos on September 1st 2011.

USO stability of 10^{-12} and is similar to two-way for an USO stability of 10^{-13} Konopliv et al., 2011).

The DTE data are related to the lander motion in space. They are thus sensitive to the revolution, the proper motion (i.e., variations of rotation and orientation of its figure), and also to the tidally driven displacement of the moon's surface. This is not the case of the ST data, which are sensitive only to rotational motion. Thus, using both data set will enable the de-correlation of the rotation from other periodical signal (especially error on body's ephemeris) in DTE data.

4. Phobos libration determination

We simulate Doppler and star tracker data using the Rambaux et al. (2012) rotational model (reported in Table 2) and following the operational scenario described in cases DTE 1 and ST 1 of Tables C1 and C2 (see Appendix C). Then we perturb the libration cosine and sine amplitudes by 20% (to match the 0.15° forced libration precision inferred by Willner et al., 2010) for the largest amplitudes, and by 100% for the smallest ones (a priori values taken as zero). In the case of the Doppler simulations, the lander position is also shifted with respect to a reference location by 1 km on the X and Y coordinates and 100 m on Z. Then we attempt to retrieve the values used to simulate the data, using least square techniques with 0.2° of a priori constraints on each amplitude (short- and long-period signals) and 10 km on X and Y, and 100 m on Z coordinates.

The results shown in the figures of this section correspond to (1) true errors, which are the absolute difference between the estimated values and the values used to simulate the Doppler data and (2) $1-\sigma$ errors or uncertainties coming from the least square inversion. They are expressed in percent of the amplitudes to be retrieved (see Table 2) or directly in degree.

For the short-period amplitudes, when the period of the libration is shorter than 1 day, the DTE Doppler solutions are more precise than the ST ones, by up to two orders of magnitude (see Fig. 1, left panel). The ST precisions of all these short-period libration amplitudes are the same and reach almost their minima relatively fast (after about 20 weeks of operations). The DTE precision of the short-period amplitudes can be divided into two families: the orbital and semi-orbital ones (dashed black curves in Fig. 1, left panel), providing the most precise solutions, and the other ones, which are on average one order of magnitude worse (solid black curves in Fig. 1, left panel). In any case, both data types lead to a precision better than 1% on W amplitudes at a 0.319 day period after only a few days of mission and DTE solutions decrease in uncertainty down to 0.001–0.01% after less than one terrestrial year of operation (see Fig. 2, right column). The small amplitudes of the W longitudinal libration at 0.5133 day are estimated at the 1% level of precision after about 50 weeks and can be retrieved with a precision of 0.5% after 100 weeks of mission by using DTE Doppler data (see Fig. 2, middle column). In α, δ, the best precisions at 0.843 and 0.2313 day are also obtained using the Doppler measurements and are at the 10% and 1% level, respectively, after about 30 weeks (see Fig. 3, two last columns).

The long-period libration amplitudes are globally more difficult to retrieve (see Fig. 1, right panel) because a longer dataset (typically one half of the period or one-third, or less, depending on the correlation between the estimated parameters) is required to improve the precision of the measurement of a long-periodic signal. For such long periodic signals, ST solutions are better than DTE solutions and their $1-\sigma$ uncertainties start to drop down more rapidly, after one-third of the period or faster, while it takes about half of the period with DTE data (see Fig. 1, right panel). This superiority of ST solutions is particularly true for W uncertainties (dashed gray curves in Fig. 1, left panel). This can be explained by the specific nature of each measurement. Indeed, ST data considered here are direct measurements of the α, δ and W angles separately (see Section 3.1). The cross-correlations are thus neglected, which is not the case for DTE observations. In addition, DTE data need to account for the unknown position of the lander, adding three parameters to the inversion, and thus requires more observing time for the de-correlation between all the parameters to be improved. The small amplitude, long-period signals can be estimated within no better than 10%, whereas the large amplitudes at a 826-day period are obtained at the 1% level, or better, on α and δ, after about 80 weeks (see Fig. 3, left column) and on W after just 30 weeks by using ST data (see Fig. 2, left column). Note that the curves drop down when sufficient data have been accumulated to improve the a priori information (see Appendix D).

A new solution of libration angle amplitudes is obtained by combining DTE and ST data. This solution is globally equivalent to the most precise individual solution. Indeed, the combined solution is as precise as the Doppler solution for short-period (<1 day period) amplitudes and is similar to the precision of the ST solutions for other periods. This demonstrates the importance of combining techniques in order to increase the science return of that type of experiments.

5. Lander localization

Together with the rotational parameters, the lander coordinates have to be estimated when one deals with DTE Doppler data (e.g., Le Maistre et al., 2012). This section presents the precision and accuracy that can be obtained on the lander location parameters.

About 50 weeks is the time needed to locate the lander at the 1 m level using DTE Doppler measurements (see Fig. 4). The centimeter level in precision on X and Y coordinates is obtained after 100 weeks of operations. The Z coordinate increases in precision of about one order of magnitude in 100 weeks, against four orders of magnitudes for X and Y. This slow increase is due to the fact that the Earth's Line of Sight (LOS) is more or less perpendicular to the Z direction, hence inducing a contribution to the Doppler (resulting from the projection of the velocity onto the LOS) quasi equal to zero (Le Maistre et al., 2012). Fig. 4 also shows on X and Y a quick decrease of the $1-\sigma$ uncertainties during the first three weeks that can be related to the very rapid estimation of the longitudinal libration in W at the orbital period (see Fig. 2, right panels). These σ_X and σ_Y quantities reach then a threshold of about 40 m, corresponding to the 0.2° of a priori error remaining on the libration at 826 days of period. Afterwards, their behavior are similar to $h_{826}=\sqrt{W_{826}^{c2}+W_{826}^{s2}}$ (see DTE 1 in Fig. C1a).

Note that, due to the difference in the magnitudes of the rotation and orientation variations between Mars (at the meter level or less) and Phobos (up to 230 m), the large a priori errors made on the POP, compared to current errors on the MOP (Mars rotation and orientation parameters, see Le Maistre et al., 2012), prevent the rapid determination of the Phobos lander location at the centimeter level, while the precise determination of the location of a lander at the surface of Mars can be achieved on a considerably faster timescale.

Finally, it is to mention that a centimeter level of precision on the lander position using DTE Doppler measurements would imply a significant improvement of the ephemeris of the Martian moon (at the same level of accuracy (see Section 6), compared against

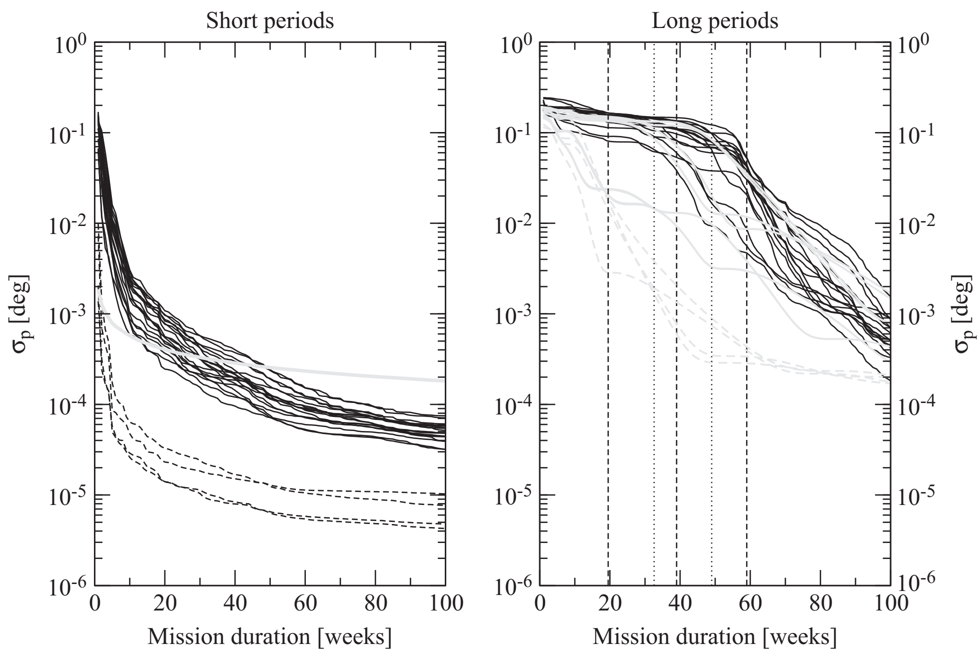

Fig. 1. 1−σ uncertainties (in degree) of all librational amplitudes estimated in this study (sin and cos amplitudes of the three angles α, δ and W denoted p in the figure) versus the mission duration. The black curves are computed from DTE data and the gray ones using ST data. The left panel shows the post-fit uncertainties for short-period signals, whose uncertainties in W at the orbital and 1/2 orbital period, obtained from DTE, are displayed with dashed lines. The right panel shows the post-fit uncertainties for long-period signals whose ST-based uncertainties in W are distinguished with dashed lines. Vertical dashed lines correspond to the sixth, third and half of the 826 day period. Vertical dotted lines correspond to the third and half of the 687 day period.

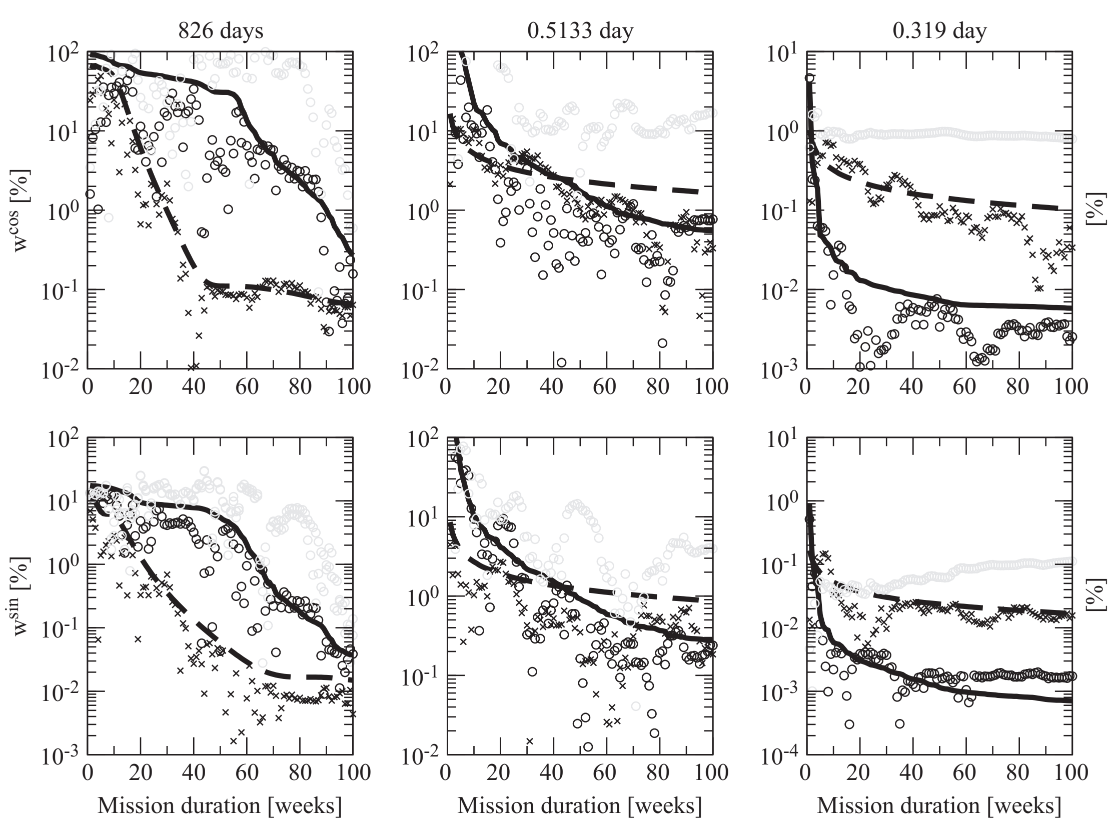

Fig. 2. Solutions in percent of the two largest amplitudes of the longitudinal libration in W and of the amplitudes of harmonic close to the resonance. Crosses and dashed curves stand for true errors and uncertainties obtained from ST data, respectively. Dots and solid curves stand for true errors and uncertainties obtained from DTE data, respectively. Black open circles have been obtained with Phobos ephemeris perturbed at the centimeter level and gray open circles with Phobos ephemeris perturbed at the meter level (see Section 6).

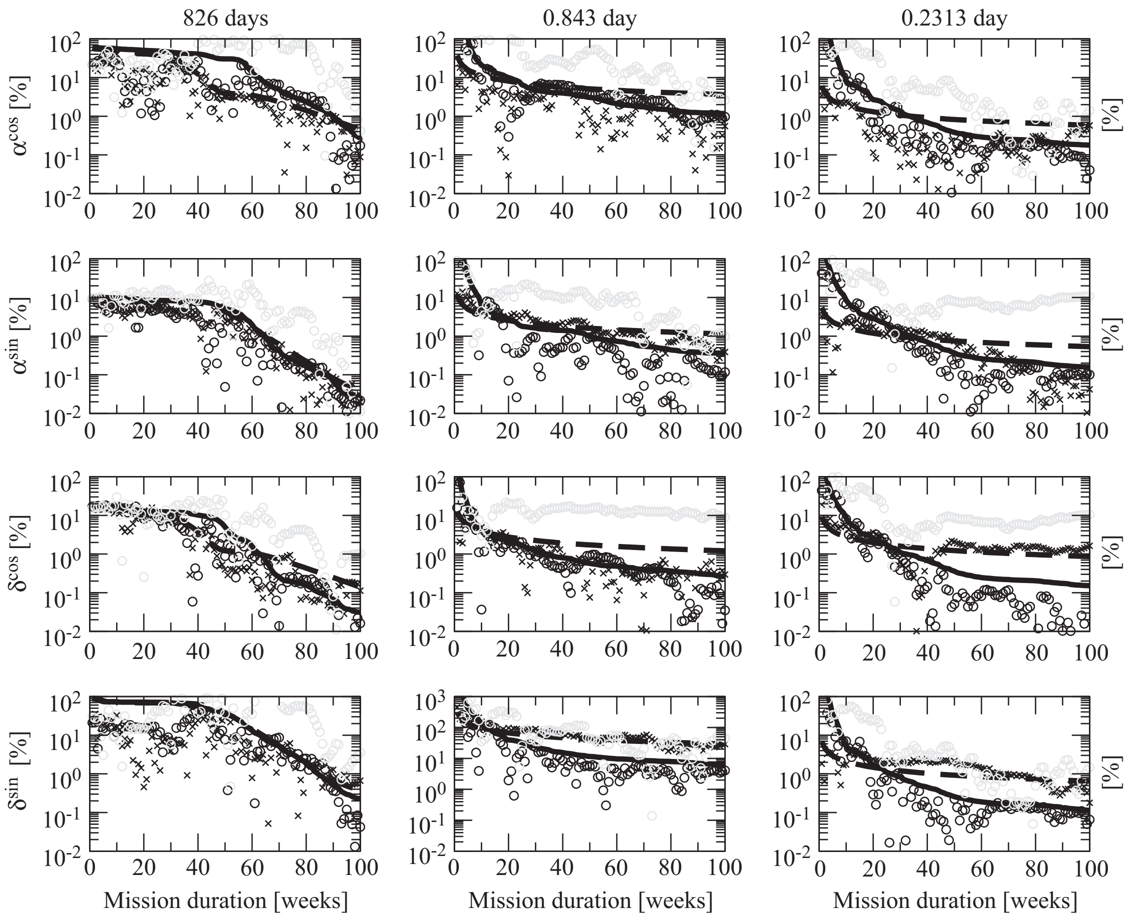

Fig. 3. Solutions in percent of the largest amplitudes and of the amplitudes of the latitudinal librations close to the resonance. Crosses and dashed curves stand for true errors and uncertainties obtained from ST data, respectively. Dots and solid curves stand for true errors and uncertainties obtained from DTE data, respectively. Black open circles have been obtained with Phobos ephemeris perturbed at the centimeter level and gray open circles with Phobos ephemeris perturbed at the meter level (see Section 6).

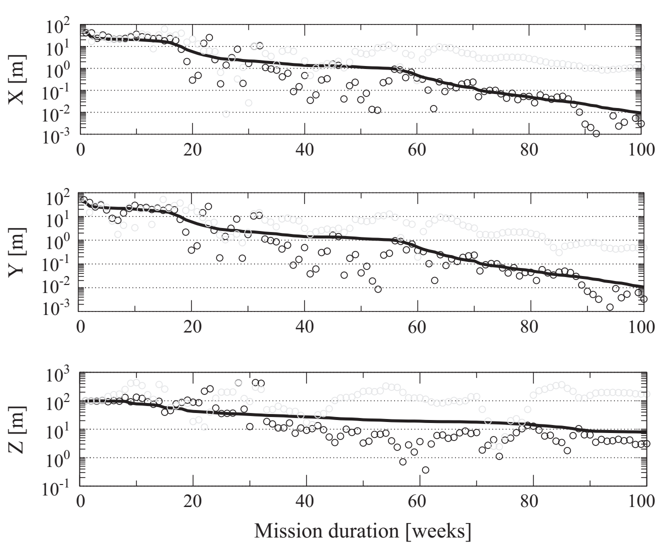

Fig. 4. Estimated lander position coordinates from DTE Doppler measurements. Solid curves correspond to 1–σ post-fit uncertainties, black open circles are true errors obtained with Phobos ephemeris perturbed at the centimeter level and gray open circles with Phobos ephemeris perturbed at the meter level (see Section 6) .

the current kilometer accuracy level Lainey et al., 2007; Jacobson, 2010), in particular if Doppler data were combined with range data to avoid any bias.

6. Phobos ephemeris issue

As pointed out in Sections 3.2 and 5, the Direct-To-Earth Doppler data track the motion of the lander in space. Therefore, these data are sensitive to variations in Phobos rotation, but also to its surface displacement due to the tides raised by Mars (see Section 11) and to its revolution around Mars. This means that errors on Phobos ephemeris will introduce biases in the libration amplitude and lander coordinates estimates. To quantify this effect on the DTE-based estimates, we have synthesized a perturbed ephemeris of Phobos at the meter level simply by rescaling the difference between Lainey et al. (2007) and Jacobson (2010) numerical ephemeris through $S_s = S_L + k(S_J - S_L)$. S_L and S_J are the state vectors provided by Lainey et al. (2007) and Jacobson (2010), respectively. S_s are the synthetical state vectors at the meter level (with a difference with S_L of about 3 m peak-to-peak in the Phobos–Earth distance), and k is the scale factor that has been chosen equal to 10^{-3}. This method has been adopted because we wanted to create ephemeris with realistic errors signatures and the meter level has been considered as realistic given the precision achieved on Mars ephemeris with similar data (Folkner, 2012). Since some proposed missions (Turyshev et al., 2010; Oberst et al., 2012) envision to strongly improve the precision on Phobos ephemeris at the centimeter level, we have also studied the impact of such a level of error on the ephemeris.

Black open circles in Figs. 2–4 stand for true errors on libration determination and lander position obtained with a Phobos

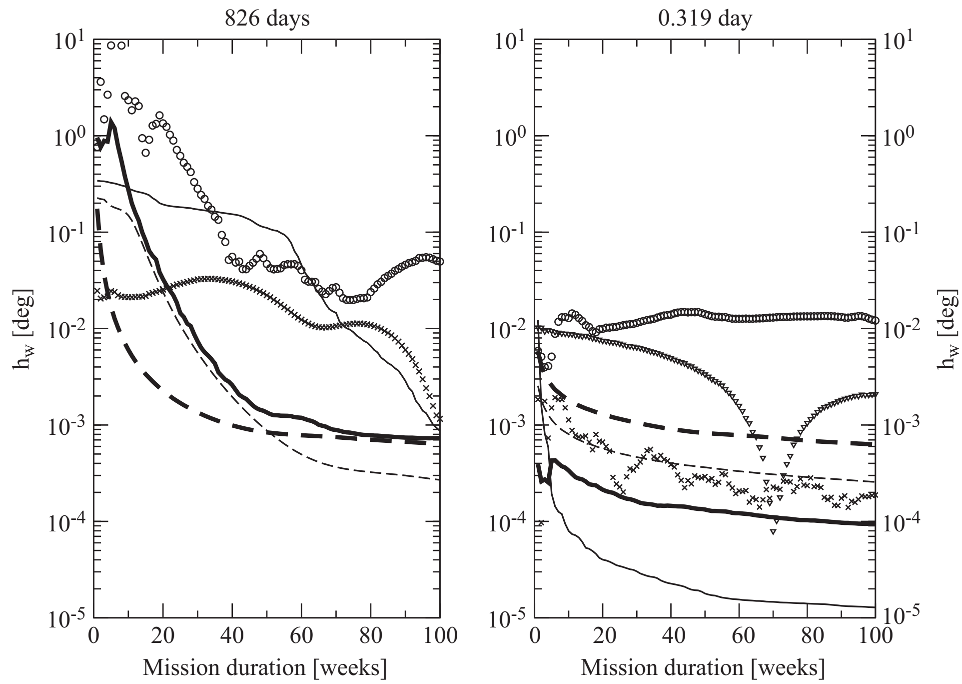

Fig. 5. Solutions obtained for the two largest amplitudes of the longitudinal libration in W (with $h_W=\sqrt{W^{c^2}+W^{s^2}}$) when estimating only the amplitudes of Seidelmann et al. (2002) from data simulated with the Rambaux et al. (2012) model. Open circles and the solid thick curves stand for true errors and uncertainties obtained from DTE data, respectively. Crosses and dashed thick curves stand for true errors and uncertainties obtained from ST data, respectively. Thin solid curves are the DTE 1 uncertainties and thin dashed curves are the ST 1 uncertainties (DTE 1 and ST 1 are defined in Appendix C and considered as the baseline in this paper). The down-pointing triangles on the right panel are true errors on W at the orbital period using ST data when a longitudinal libration in W, with an amplitude of 10^{-2} degree and a period very close to 0.319 day, is ignored. See text for details.

ephemeris at the centimeter level. These biases in the estimates exhibit very similar behavior as with non-perturbed Phobos ephemeris. This can be explained by the fact that the smallest signal to be retrieved is greater than 2 cm as noticed in the caption of Table 2.

Gray open circles in Figs. 2 and 3 are the true errors on libration determination obtained with a Phobos ephemeris at the meter level. We see the consequences of such an error on libration estimates with DTE Doppler data. Roughly, the long-period needs about 25 additional weeks to be measured with similar accuracy than with a perfectly known ephemeris. Most of the short-period librations amplitudes show significant biases. In particular, the longitudinal libration at the orbital period presents steady biases where true errors remain at about 0.001°, i.e., about 20 cm. Nevertheless, even with such ephemeris error, the orbital libration amplitude accuracies are still better than 1%. Fig. 4 shows that the true errors on X and Y lander coordinates are at the level of the Martian moon ephemeris error.

In conclusion, error in bodies ephemeris is one of the major concern in the processing of DTE Doppler data. This implies that lander coordinates, librational motion and orbital motion will have to be solved jointly or iteratively, otherwise parameters solutions will be significantly biased. As stated before, a combined experiment with star tracker and Doppler data offers useful way to de-correlate the contributions of the ephemeris and of the librations in the Doppler data since ST data do not depend on the ephemeris. One cannot exclude that, perhaps, another kind of experiment would be more appropriate to de-correlate the parameters using for example several landers and radio sources available at the surface of Phobos or by using an additional radio link between the lander and an orbiter around Phobos, the latter link not being sensitive to the states of the moon. Nevertheless, the proposed approach should be one of the less difficult and expensive one and then may be a good first step.

7. Phobos rotation mis-modeling

In this section we perform simulations to assess the impact of a mis-modeling (e.g., non-estimated amplitudes) in the ST and DTE data reduction process. Starting with the Phobos libration amplitudes of Seidelmann et al. (2002) (involving only the 826-days and 0.319-day periodic signals) and adjusting only these amplitudes on the simulated data based on the model of Rambaux et al., 2012, the inferred solutions are very biased (see true errors, crosses and dots, in Fig. 5 with respect to the uncertainties, solid and dashed curves), indicating that the post-fit uncertainties are then too optimistic. We note, however, that we reach the 10% precision level for the long period libration amplitude and that true errors and uncertainties remain below 10^{-2} degree ($<1\%$) for the orbital period libration amplitude, still offering a relevant insight into the interior of Phobos (see the following sections).

We also take a look at the effect of small amplitude signals with a period very close to one of the period considered in Table 2. We create data with one more longitudinal libration of amplitude $h_W=10^{-2}$ degree and period 0.3188 day, which is very close to the orbital period libration. We then estimate all the amplitudes reported in Table 2 as done earlier, intentionally forgetting this new fictitious libration. The post-fit uncertainties remain the same but the amplitudes estimated for the 0.319-day libration are very biased as shown by the down triangles in the right panel of Fig. 5. We see, however, that these true errors exhibit a peculiar behavior, where the additional error induced by the ignored signal totally vanishes after 72 weeks before appearing again. It turns out that true errors on $h_{W_{0.319}}$ have a periodical behavior with an amplitude equal to that of the neglected libration (here 10^{-2} degree) and with a period equal to the synodic period between the period of the signal under consideration (here $T_k=0.319$ day) and the period of the ignored signal (here $T_u=0.3188$ day), i.e., a period equal to $T_s=\|1/(1/T_k-1/T_u)\|\simeq 72$ weeks in this example. In other words, a forgotten librational component with amplitudes greater than the truncation level[3] and period close to one used in the model will be detected and characterized (amplitude, frequency and phase) by its signature on the amplitude estimated for the modeled signal. Moreover, this analysis shows that, even if such a signal is neglected, the longitudinal libration at the orbital period can still be estimated at least at the percent level, providing tight constraints on the mass distribution inside Phobos (see the following sections).

8. Phobos' proper modes

In the previous section, we showed that the librational motion of Phobos can be measured with a very high precision of 10^{-3}–10^{-5} degree depending on the period of the estimated signal with respect to the mission duration. Now we describe the relationship between the librational measurements and the proper modes of Phobos and we infer the precision that could be obtained on the latter from a *Phobos-Soil* like mission.

We note that most of the numerical calculations done hereafter are built on approximated values (see Table 3), the goal here being to provide some orders of magnitudes of the physical parameters precisions that can be estimated from future measurements.

The free (or proper) librations around the equilibrium are assumed to be damped and there is no stimulated mechanism at these frequencies. However, it is important to know their frequencies, because they characterize the way the system reacts to external sinusoidal excitations, which are mainly caused here by the variations of the distance between Mars and Phobos. Moreover, the proper modes depend on the moments of inertia (MOI) values (Chapront-Touzé, 1990), which are crucial values to constrain the interior of Phobos (see Section 9).

Precise estimates of the amplitudes of libration could thus provide constraints on the proper modes of Phobos and therewith on its MOI. Since the signature of interior properties on the libration amplitude is increased when proper and forcing frequencies are close to each other (resonance), we first look for the possible existence of resonant cases given the MOI values of the Martian moon quoted in the literature. The range of proper frequencies that match the interior models of Duxbury (1989), Borderies and Yoder (1990) and Willner et al. (2010) are reported in Table 4.

ν_L and ν_W are latitudinal and wobble modes of the rotation, respectively, as defined in Chapront-Touzé (1990) and Rambaux et al. (2012). The longitudinal proper mode, ν_τ, is defined as a function of the relative moment of inertia γ as follows (Chapront-Touzé, 1990):

$$\nu_\tau = n\sqrt{3\gamma}, \tag{12}$$

where $n = 2\pi/0.319$ rad/day is the mean motion of Phobos. Setting $A \le B \le C$ the MOI of Phobos, γ and the other two relative moments of inertia ζ and β can be defined as

$$\zeta = \frac{C-B}{A}, \tag{13}$$

$$\beta = \frac{C-A}{B}, \tag{14}$$

$$\gamma = \frac{B-A}{C}. \tag{15}$$

[3] If the neglected signal has an amplitude smaller than the truncation level (here equal to 10^{-4} degree) it will be undetectable because it will have no influence on the determination of the other parameters.

Looking at Tables 2 and 4, it appears that resonance scenarios are possible as noted by Chapront-Touzé (1990). Indeed, among the forcing periods of Table 2, T=0.5133 day (corresponding to $\omega_T = 2\pi/T \simeq 12.24$ rad/day) is within the range of ν_τ and thus can be very close to the longitudinal proper frequency of Phobos.[4]

In addition, resonances are possible with the latitudinal and the wobble proper modes since $\omega_{T=0.2313} \simeq 27.16$ rad/day is around $\nu_L \in [27.26, 27.82]$ rad/day, and $\nu_W \in [7.41, 8.72]$ rad/day includes $\omega_{T=0.843} \simeq 7.45$ rad/day.

We focus in this study on the main libration in longitude (at the orbital period and at 826 days) and on the libration close to the resonance through a linear approach. It has been shown (e.g., Danby (1988); Borderies and Yoder (1990); Chapront-Touzé (1990)) that, at first order in eccentricity and in librational amplitude, the non-linear differential equations describing the rotational motion of a body in synchronous spin-orbit resonance might be linearized, providing a good first order approximation for the libration angle.[5]

In response to a periodic forcing decomposed as $\sum_T H_T \sin(\omega_T t + \varphi_T)$, where H_T represents the magnitude of the forcing, ω_T and φ_T represent its frequency and phase, respectively (neglecting the impact of the quadratic evolution of the libration), the libration angle in longitude τ is expressed in Fourier series as

$$\tau = \sum_T h_T \sin(\omega_T t + \varphi_T). \tag{16}$$

The phase φ_T of τ is equal to that of the periodic forcing, but the amplitude h_T is modulated by the interior structure of the moon following:

$$h_T = \frac{\nu_\tau^2}{\nu_\tau^2 - \omega_T^2} H_T. \tag{17}$$

T is the period of the considered libration and $\omega_T = 2\pi/T$ is the forcing pulsation. We note that H_T at the orbital period is $H_{0.319} = 2e$, with e the orbit's eccentricity of Phobos leading to the classical expression of the libration amplitude (e.g., Eq. (2) in Willner et al., 2010).

We now look at the relationships between the librational amplitudes, h_T, and the proper mode, ν_τ, of Phobos for the three oscillations with $T \in \{0.319, 0.513, 826\}$. h_{826} is quasi-constant ($\Delta h_{826} \simeq 10^{-8}$ degree), which means that the long-period amplitudes (with $\omega_T \ll \nu_\tau$) have almost no contribution from the proper mode and thus are not sensitive to the relative moment of inertia $(B-A)/C$. This can be easily deduced from Eq. (17) where the dependency on ν_τ disappears with increasing period T ($\omega_T \to 0$, implying that $\nu_\tau^2/(\nu_\tau^2 - \omega_T^2) \to 1$). This results has been quoted in the numerical analysis of Rambaux et al. (2012, Table 9), in which the amplitudes of long period oscillation (low frequency) are almost constant whatever the interior model. Note that these long period librations are thus equal to the orbital variations ($h_T = H_T$). Hence, a precise estimate of their amplitudes will provide additional constraints in the computation of the ephemeris of the moon. The librational amplitude at the orbital period, far from the resonance, varies strongly and linearly within 0.4° given the range of ν_τ. Finally the amplitudes at 0.513 day can be very large if we are exactly at the resonance, but this amplification effect is very localized (in a narrow range of ν_τ). However, in such a case, the linear model used here is not accurate enough and analytical development at higher order are required (as in Chapront-Touzé, 1990) or a numerical approach as in Rambaux et al. (2012).

[4] Note that the W amplitude of this period does not comes from the amplitude of τ, which remains small despite the proximity with ν_τ (Rambaux et al., 2012), but comes in fact mainly from the second term $-\Delta\alpha \sin\delta$ in Eq. (18).

[5] Borderies and Yoder (1990) and Chapront-Touzé (1990) investigated the non-linear effects in detailed analytical studies and Rambaux et al. (2012) studied their consequences through a numerical approach.

Table 3
Physical and dynamical properties of Phobos and Mars (primed quantities) used in the calculations.

Parameter	Symbol	Value	Unit
Phobos			
Mean radius[a]	R_0	10.956	km
Mean radius[b]	R	11.27	km
Mean equatorial radius[c]	R_e	12.22	km
Semi-major axis[d]	R_a	13	km
Semi-medium axis[d]	R_b	11.39	km
Semi-minor axis[d]	R_c	9.07	km
Mass[e]	M	1.06×10^{16}	kg
Density[e]	ρ	1875	kg/m^3
Degree-3 gravity coef[f].	C_{31}	−0.00236	–
	C_{33}	0.00018	–
Orbit eccentricity[h]	e	0.01511	
Orbit semi-major axis[h]	a	9375	km
Mars			
Mass[g]	M'	6.42×10^{23}	kg
Reference radius[g]	R'	3396.0	km

[a] Used by Willner et al. (2010) to normalize the MOI.
[b] $R^2=(R_a^2+R_b^2+R_c^2)/3$.
[c] $R_e^2=(R_a^2+R_b^2)/2$.
[d] From Willner et al. (2010).
[e] From Andert et al. (2010).
[f] From Borderies and Yoder (1990).
[g] From Konopliv et al. (2006).
[h] From Jacobson (2010).

Table 4
Phobos moments of inertia (A,B,C) from three different publications and the inferred degree-two gravity coefficients (C_{20},C_{22}), relative moments of inertia (ζ,β,γ) and proper modes (ν_τ,ν_L,ν_W). In these references, MOI data have been computed from shape radii assuming constant density. For comparison, the MOI values shown in this table have all been normalized using R_0 reported in Table 3.

Parameter	Borderies and Yoder (1990)	Duxbury (1989)	Willner et al. (2010)	Unit
A/MR_0^2	0.3570	0.3371	0.3615	–
B/MR_0^2	0.4248	0.3881	0.4265	–
C/MR_0^2	0.4979	0.4785	0.5024	–
I/MR_0^2	0.42656	0.40123	0.43013	–
C_{20}	−0.1070	−0.1159	−0.1084	–
C_{22}	0.01695	0.01275	0.01625	–
ζ	0.204762	0.268170	0.209958	–
β	0.331685	0.364339	0.330363	–
γ	0.136172	0.106583	0.129379	–
ν_τ	12.589068	11.137659	12.271049	rad/day
ν_L	27.303633	27.818855	27.261108	rad/day
ν_W	7.405864	8.718200	7.495965	rad/day

We describe the rotation of Phobos using (α,δ,W) coordinates. These angular coordinates are connected to τ as follows (Konopliv et al., 2006):

$$\Delta W=\tau-\Delta\alpha\ \sin\ \delta, \tag{18}$$

where ΔW and $\Delta\alpha$ correspond to the trigonometric series in Eqs. (3) and (1), respectively.[6]

Then, the precisions obtained on α,δ and W in Section 4 are propagated on h_T using Eqs. (16) and (18).

We are now able to infer the precision on the proper frequency from the precision achieved on the determination of h_T after less than 10 weeks of DTE and ST operations (see Section 4), by computing

$$\sigma_{\nu_\tau}(T)=\frac{(\nu_\tau^2-\omega_T^2)^2}{2\nu_\tau\omega_T^2}H_T^{-1}\sigma_{h_T}. \tag{19}$$

The behavior of the uncertainties σ_{ν_τ} for the librations at the orbital period $T=0.319$ day and the libration at $T=0.513$ day are shown in Fig. 6 as a function of the proper frequency value ν_τ. Because of the quasi-linear relationship between the $h_{0.319}$ amplitude and ν_τ, σ_{ν_τ} depends very weakly (i.e., slow decrease when the proper frequency increases) on the actual value of ν_τ when using solutions of orbital period amplitudes. In contrary, σ_{ν_τ} varies strongly given the value of ν_τ when using solutions of h_T at 0.513 day and can drop to 10^{-8} rad/day or smaller if ν_τ is very close to the forcing frequency. However, as shown on Fig. 6, $\sigma_{\nu_\tau}(0.513)$ is more interesting than $\sigma_{\nu_\tau}(0.319)$ (i.e., $\sigma_{\nu_\tau}(0.513)<\sigma_{\nu_\tau}(0.319)$) only if ν_τ is within the narrow range: $[12.228, 12.253]$ rad/day. We should have about $\sigma_{h_{0.513}}<10^{-3}\sigma_{h_{0.319}}$ to reverse this situation and make $h_{0.513}$ systematically the most interesting amplitude to be used for improving our knowledge on ν_τ. Using the most recent value of the MOI (Willner et al., 2010) in Eq. (19) yields $\nu_\tau=12.271049\pm0.52$ rad/day. For this value, $\sigma_{h_{0.513}}\approx6\sigma_{h_{0.319}}$, which is just outside from the latter range. However, we cannot exclude the resonance scenario considering the large error bar (±0.52 rad/day) inferred from the libration precision of Willner et al. (2010) ($\sigma_{h_{0.319}}=0.15^\circ$).

We conclude that longitudinal libration amplitudes at the orbital period, while being clearly distinct from the resonance period, will certainly provide the best precision on ν_τ ($\approx3.5\times10^{-4}$ rad/day after about 10 weeks and up to $\approx3.5\times10^{-5}$ rad/day after about one Earth year of mission duration).

9. Phobos' MOI

In this section we assess the precision that can be inferred on Phobos MOI from its proper mode estimates showing the great interest of DTE and ST experiments as avenues to constrain the interior structure of Phobos. Internal structure is one of the keys in the search of origin (Rosenblatt, 2011).

The uncertainty on the relative difference in the MOI, γ, can be computed from the free frequency value and uncertainty by using (as derived from Eq. (12))

$$\sigma_\gamma=\frac{2}{3}\frac{\nu_\tau}{n^2}\sigma_{\nu_\tau}. \tag{20}$$

Thus it is found that the value of σ_γ is about 50 times smaller than the value of σ_{ν_τ}, reaching 7×10^{-6} after 10 weeks of operation and 7×10^{-7} after one Earth's year.

Even with such a high precision on γ, and even if we assume a similar precision on ζ and β, inferring the precision on A, B, and C remains difficult, because of the non-linearity of Eqs. (13)–(15). By using a direct approach, based on a Monte Carlo error propagation, we can successfully derive the main MOI with a precision no better than 10% (quasi-independently from the actual precision on ζ, β, γ).

The potential departure from homogeneity of Phobos' interior is still under study. Rambaux et al. (2012) have proposed a heterogenous model with a contrast in density of about 30% between the region of Stickney and the rest of the body, based after earlier models for the origin of Stickney (e.g., Asphaug and Melosh, 1993). This configuration shifts the MOI by less than 10% from the homogenous value (see Rambaux et al. (2012, Table 1)), in order to be consistent with the observed amplitude of the libration by Willner et al. (2010).

By discretizing the volume of Phobos into about 135 000 cubes of equal volume (~350 m^3) corresponding to material of either silicate, porous silicate and water ice, and by fitting the bulk

[6] Note that in the case of orbital and sub-orbital librations, $\Delta W\approx\tau$, since $\Delta\alpha\approx0$ (see Table 2 for W and Table 5 for τ in Rambaux et al., 2012).

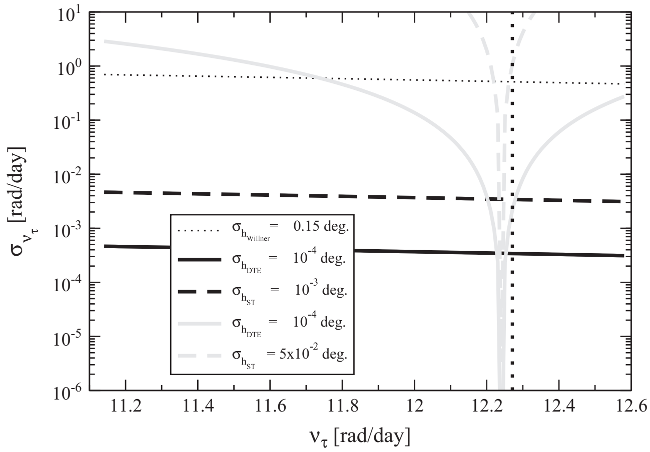

Fig. 6. Inferred uncertainty on ν_τ as a function of its own value after 10 weeks of mission. Gray curves are obtained using ST (dashed) and DTE (solid) uncertainties on $h_{0.513}$ and black curves are obtained using ST (dashed) and DTE (solid) uncertainties on $h_{0.319}$. The vertical thick dotted line is the mean value of ν_τ derived from Willner et al. (2010) MOI. The horizontal thin dotted line is σ_{ν_τ} derived from the libration precision of 0.15° obtained by Willner et al. (2010).

density and the observed libration, Rosenblatt et al. (2010, 2011) have found that Phobos is probably heterogenous and that its MOI departs from the homogenous value by less than 5%. Hence, the obtained precision on the MOI ($>10\%$) is still insufficient for constraining the global interior properties of Phobos (homogenous versus heterogenous in composition and porosity) above all because the above-cited levels of departure (5–10%) are for extreme models, whereas the most abundant models change the MOI by ~1% or even less.

Nevertheless, a precise estimate of the degree-two gravity coefficients C_{20} and/or C_{22} would also contribute to increase the precision on the MOI, since they are related to the moments of inertia (taking normalized A, B, C) by

$$C_{20} = \frac{B+A}{2} - C, \tag{21}$$

$$C_{22} = \frac{B-A}{4}. \tag{22}$$

Since the *Phobos-Soil* mission failed, the only current candidate that could be used to estimate Phobos degree-two gravity field is *Mars Express* during a future close flyby. However, the polar orbit of MEX prevents flybys in the equatorial plane of Phobos so that C_{20} could be more easily determined than C_{22} because of its larger induced MEX orbital perturbations. We thus consider in our study the normalized A, B and C as functions of ζ, β, γ and of C_{20} and C_{22} separately

$$A = 4C_{22}\left(\frac{\beta-1}{\zeta-\beta}\right), \tag{23}$$

$$B = 4C_{22}\left(\frac{\zeta-1}{\zeta-\beta}\right), \tag{24}$$

$$C = \frac{4C_{22}}{\gamma}, \tag{25}$$

and

$$A = \frac{2(1-\beta)}{2\zeta\beta-\zeta-\beta} C_{20}, \tag{26}$$

$$B = \frac{2(1-\zeta)}{2\zeta\beta-\zeta-\beta} C_{20}, \tag{27}$$

$$C = \frac{2(1-\zeta\beta)}{2\zeta\beta-\zeta-\beta} C_{20}. \tag{28}$$

From the above equations, we can infer the uncertainties on A, B, and C as a function of the uncertainties on the relative moments of inertia[7] and of $\sigma_{C_{20}}$ or $\sigma_{C_{22}}$.

σ_A and σ_B behave similarly as σ_C, which is why we have only represented the latter on Fig. 7. Taking $\sigma_\gamma = 10^{-5}$ as expected after about 10 weeks of mission duration, and assuming that $\sigma_\zeta = \sigma_\beta = 10^{-4}$ (to be checked in future work), we see that C_{20} and C_{22} yield similar precision on C and that σ_C is equal to $\sigma_{C_{2x}}$ down to the precision of 0.1%. The 1% level of precision on A, B and C is reached for a precision of 1% on the gravity coefficient C_{20} or C_{22}.

This shows that both the relative MOI and one of the gravity coefficients needs to be determined at the percent level or better in order to infer from the MOI the degree of departure from a homogenous interior. Note that the current precision on the A, B, C for an homogenous interior equals 2% if one propagates the volume error of 60 km^3 obtained by Willner et al. (2010) on the MOI. This means that the current error on the homogenous values of A, B and C do not prevent to detect the heterogenous interior signature in the MOI if it is large, but to observe a signature smaller than 1% both the MOI and the volume of Phobos have to be improved.

10. Phobos gravity field and Mars oblateness

As presented in the previous sections and well illustrated by known Eqs. (21) and (22), the degree-two gravity field is intimately linked to the MOI and therefore to the short-period amplitudes of librations. Furthermore, the librations of Phobos are also perturbed by its degree-three gravity field and Mars' oblateness. Rambaux et al. (2012) have shown that these perturbations are expected to modulate the librational amplitudes especially that at the orbital period (by about 0.03% and 0.1% respectively), because of its large amplitude, and that at the 0.513-day period (by about 15% and 34%, respectively) because of the proximity to the resonance. Even if the increase at the orbital period appears to be small, the very precise measurements of $W^{c,s}_{0.319}$ will allow the detection of these contributions in less than 10 weeks (see Fig. 2, right panel). The signature of Phobos' degree-three gravity field and that of Mars oblateness on the longitudinal libration amplitudes obtained by Rambaux et al. (2012) can be related to the modification of the free frequency ν_τ (see their Eqs. (13) and (14)) . Thus, the precision on C_{31} and C_{33} Phobos' gravity coefficients can be inferred from σ_{ν_τ} given the fact that $\sigma_{C_{31}} = 90\sigma_{C_{33}}$ and that

$$\sigma_{C_{33}} = \frac{2}{135}\frac{C}{n^2}\frac{a}{R}\nu_\tau \sigma_{\nu_\tau}. \tag{29}$$

After a 100-week mission duration, we obtain $\sigma_{C_{33}} \simeq 6.3\times10^{-6}$ and $\sigma_{C_{31}} \simeq 5.7\times10^{-4}$, corresponding to 3.5% and 14% of their own value, respectively.[8]

The uncertainty on Mars J_2 is estimated at about 10^{-5} inserting the numerical values of Table 3 in the following equation:

$$\sigma_{J_2} = \frac{4}{15}\left(\frac{a}{nR'}\right)^2 \frac{\nu_\tau}{\gamma}\sigma_{\nu_\tau}. \tag{30}$$

Such a precision is not sufficient to improve our knowledge of the Martian oblateness (current precision is of order of its seasonal

[7] Since we have $\zeta\beta\gamma = \zeta - \beta + \gamma$, it is easy to show that γ is present in the expressions of A and B as a function of C_{22} and in the expression of C as a function of C_{20}.

[8] Note that C is considered in Eq. (29) as well known and that a C value known at the 1% level would increase $\sigma_{C_{33}}$ by about 5%.

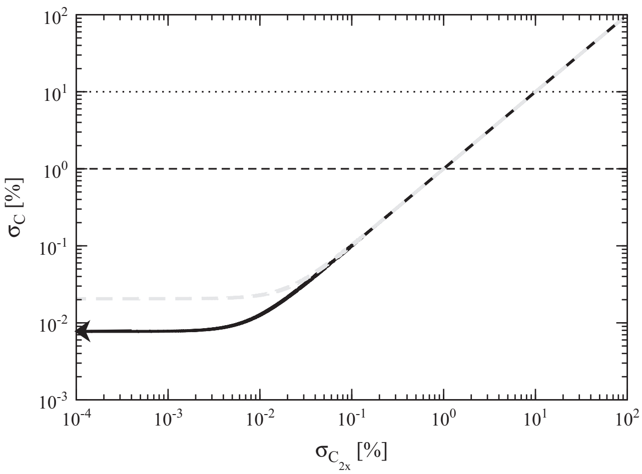

Fig. 7. Inferred uncertainties on the polar moment of inertia (in %) as a function of the precision on C_{20} (thick gray dashed curves) and C_{22} (thick black solid curves) from assumed precisions on ζ, β (10^{-4}) and from the predicted precision on γ (10^{-5}) obtained after 10 weeks of mission duration. Thin horizontal dotted line corresponds to the actual 10% level of precision and thin horizontal dashed line is the target precision in order to be conclusive on the homogeneity/heterogeneity of Phobos. The arrow shows the σ_γ/γ value.

variations, $\Delta J_2 \approx 10^{-9}$ Konopliv et al., 2006, 2011; Marty et al., 2009). In any case, accounting for the degree-three gravity field of Phobos yields exactly the same precision on γ as obtained before (Eq. (20) remains valid) whereas uncertainty in Mars' J_2 degrades σ_γ by only 0.06%.

In summary, one could expect from these experiments to infer the proper mode ν_τ and so the relative moment of inertia γ with a precision better than 0.005% after only 10 weeks of operation.

11. Phobos' rigidity and tidal deformation

The tidal potential induced by Mars on Phobos causes a diurnal tide, i.e., periodic variations in surface displacements. The lander DTE measurements are sensitive to this surface displacement and could therefore be used to put constraints on the ability of Phobos to deform in response to tidal forcing, a property expressed by the Love number h_2. In this section we quantify this displacement and compare it against the measurement accuracy predicted by the simulations.

While Phobos' surface properties have been imaged multiple times and with relatively high resolution (e.g., Thomas et al., 2011), we lack constraints on its composition and internal structure. The tidal Love numbers are primarily functions of the viscoelastic properties of the material, i.e., its shear and bulk moduli, as well as density. The elastic properties of the material are determined by composition and porosity fraction. Unfortunately, considering the uncertain the bulk composition of the moon, the parametric space describing these two properties is broad and loosely bounded. Indeed, Phobos' composition ranges from high-density anhydrous silicate with up to 45% porosity to a carbonaceous chondrite (grain density of 2.1 g/cm^3 offset by 10% porosity, Rosenblatt, 2011; Murchie et al., 2013). The presence of few ice has also been proposed to explain Phobos' relatively low density (Fanale and Salvail, 1989; Rosenblatt et al., 2011), in which case Phobos' interior would be a mostly homogenous mixture of ice and rocks. Depending on porosity, Phobos may be a monolith (unlikely, see Rosenblatt, 2011), a moderately porous object, or a rubble-pile.

The (unrelaxed) shear modulus of material grain, μ, may range from 10^9 Pa (Lambeck, 1979) to 10^{11} Pa. In the present study we consider a broad parametric space that covers uniform elastic solid body to a rubble-pile body.

Following Goldreich and Sari (2009), we define the dimensionless rigidity $\tilde{\mu}$ for a spherical homogenous incompressible body as

$$\tilde{\mu} = \frac{19}{2}\frac{\mu R}{\rho G M}, \tag{31}$$

where G is the gravitational constant, ρ is its mean density and R is its mean radius (see Table 3 for the numerical input). Neglecting material compressibility impacts the value of $\tilde{\mu}$ by less than 7.5% (pers. com. from Rivoldini A. January 2012). The above equation has been defined for a homogenous body in hydrostatic equilibrium. However, Phobos' shape is not hydrostatic and its interior is likely to exhibit some lateral variations in density. We lack constraints on the interior properties and methodology to measure the impact of large departure of hydrostaticity on the calculation of h_2. Hence the following discussion is based on establishing orders of magnitude for potential observables expressing Phobos' tidal response.

Assuming a rubble-pile (i.e., no cohesion), Goldreich and Sari (2009) have shown that the quantity $\tilde{\mu}_{rubble}$ is in the range

$$\sqrt{\frac{\tilde{\mu}}{\epsilon}} \le \tilde{\mu}_{rubble} \le \tilde{\mu}, \tag{32}$$

where ϵ stands for the material's yield strain ($\approx 10^{-2}$, Goldreich and Sari, 2009), and the lower bound corresponds to a rubble-pile composed of irregular elements. In the rest of the paper, we will denote $\tilde{\mu}_{rubble}$ as being equal to this low endmember value $\sqrt{\tilde{\mu}/\epsilon}$.

From the numerical calculation it appears that $\tilde{\mu}_{rubble}$ is 1–2 orders of magnitude smaller than $\tilde{\mu}$ and that $\tilde{\mu}$ can vary by two orders of magnitudes depending on composition. Since, at first order, $\tilde{\mu}$ is related to the tidal Love numbers through

$$h_2 = \frac{5}{2}(1+\tilde{\mu})^{-1}, \tag{33}$$

$$k_2 = \frac{3}{2}(1+\tilde{\mu})^{-1}, \tag{34}$$

these two coefficients also fall within orders of magnitude reported in Table 5. Note that these ranges obtained under the assumption that the body is incompressible would be slightly different (by less than 1% with $\mu = 1$ GPa and less than 10% with $\mu = 100$ GPa for h_2, e.g., Hurford and Greenberg, 2001) by accounting for material compressibility. Also, accounting for the very non-spherical shape of Phobos will introduce in h_2 a shifting term function of latitude ϕ (e.g., Petit et al., 2010)

$$h_2 = h_2^{sphere} + \check{h}_2[(3\,\sin^2\phi - 1)/2]. \tag{35}$$

However, the second term in the right hand side of Eq. (35) remains less than 20% of h_2^{sphere} as it is proportional to the deviation from sphericity.

Finally, the tidal radial displacement, Δr, can be calculated since it is related to h_2 through

$$\Delta r = h_2 \frac{V_t}{g}, \tag{36}$$

where V_t is the tidal potential and g is the gravitational acceleration at the surface of Phobos. For a synchronous satellite like Phobos, the maximum value of V_t/g is equal to

$$\left|\frac{V_t}{g}\right| = 3\frac{M'}{M}\frac{R^4}{a^3}e, \tag{37}$$

where M' is the mass of Mars, M is the mass of Phobos, a is the semi-major axis and e is the eccentricity of its orbit (see Table 3 for the list of input parameters). We note that the quantity $|V_t/g|$ can vary, depending on the R used value, from single ($\approx$47.6 m with the R_0) to double ($\approx$94.4 m with R_a). Consequently, the amplitude

Table 5
Ranges of values of rigidity and of quantities related to the tides on Phobos computed with $R = 11.27$ km.

Quantity	Range	Unit
μ	$[10^9; 10^{11}]$	(Pa)
Monolithic body		
$\tilde{\mu}$	$[8.1\times10^4; 8.1\times10^6]$	–
h_2	$[3.1\times10^{-7}; 3.1\times10^{-5}]$	–
k_2	$[1.84\times10^{-7}; 1.84\times10^{-5}]$	–
Δr	$[1.65\times10^{-3}; 0.165]$	cm
Rubble pile body with $\epsilon = 0.01$		
$\tilde{\mu}_{rubble}$	$[2.85\times10^3; 2.85\times10^4]$	–
$h_{2_{rubble}}$	$[8.8\times10^{-5}; 8.8\times10^{-4}]$	–
$k_{2_{rubble}}$	$[5.3\times10^{-5}; 5.3\times10^{-4}]$	–
Δr_{rubble}	$[0.47; 4.7]$	cm

of the tidal deformation that can be calculated from Eqs. (36) and (37) can also vary by a factor two given the value of the radius taken into account.[9] We have chosen to use the mean radius R in our numerical calculations (see Table 3), implying $|V_t/g| = 53.3$ m. We draw from this choice that the position of the lander with respect to the center of mass of Phobos could vary by up to 5 cm at the orbital period.

In summary, given the broad parametric space considered, we have been able to calculate plausible ranges of quantities related to the tides that are reported in Table 5.

We have then estimated the precision that can be achieved on the determination of the Love number h_2 from DTE Doppler data, adding then a 42nd parameter to be determined. This new parameter appears to be poorly correlated with the others, therefore not perturbing significantly their determination (i.e., expected precisions on the POP and lander coordinates shown in the previous sections still hold). The post-fit true errors and uncertainties obtained on h_2[10] are shown in Fig. 8, left y-axis. σ_{h_2} does not depend on the value of h_2, because Eq. (36) is linear in h_2. This means that the precision that will be obtained on this parameter from DTE Doppler data will remain that shown in Fig. 8, whatever the nature of Phobos (monolithic or rubble-pile), and thus whatever the effective value of Phobos' h_2 (in the ranges of Table 5). These uncertainties have been propagated on the tidal displacement Δr (Fig. 8, right y-axis) with the expected ranges of surface displacements of Table 5. We see that the tidal surface displacements of a rubble-pile Phobos could be observed from DTE Doppler data, assuming Phobos ephemeris known at the centimeter level, after only 20 weeks of operation if Phobos is composed of carbonaceous chondrite and in less than 70 weeks if it is made of silicate. Moreover, we see that a uniform elastic Phobos composed of carbonaceous material (with $\mu = 1$ GPa) will display tides that will be barely observed with DTE Doppler data if the tracking duration is greater than a Martian year, whereas they will not be detected in case of a silicate monolithic Phobos (with $\mu = 100$ GPa).

In summary, DTE Doppler experiment will put constraints on the nature of Phobos's interior (rubble-pile or monolith) in less than a Martian year, providing therefore new insight on the origin and evolution of this moon (Rosenblatt, 2011). However, this prediction is contingent upon the position and velocity of Phobos being known at the centimeter level. Since the h_2 signal is correlated with the ephemeris error, and even if the signature of h_2 on the Doppler could be up to four times the data noise level of 0.05 mm/s at 60 s of integration time, the true errors increase when the accuracy of the ephemeris decreases. This is shown in Fig. 8 where black and gray dots are obtained with ephemeris at centimeter and meter level of accuracy, respectively. Hence, to avoid bias in the tidal displacement estimates, the Phobos' ephemeris will have to be dramatically improved below the centimeter level of accuracy. This can be done by a dedicated mission like *GETEMME* (Oberst et al., 2012) or *PLR* (Turyshev et al., 2010) that involve Laser measurements and predict a millimeter level of range resolution. Finally, systematic effects due to antenna cables or thermal deformation of the antenna itself could occur and overwhelm the tidal signal. Nevertheless, such behavior of the payload hardware should be precisely modeled by the engineer team of the mission and then removed from the data.

Now, we propagate the uncertainties in h_2 on μ by calculating

$$\sigma_\mu = \frac{5}{19}\frac{\rho GM}{Rh_2^2}\sigma_{h_2} \simeq \frac{4}{95}\frac{\rho GM\tilde{\mu}^2}{R}\sigma_{h_2}. \tag{38}$$

Firstly, we note that, considering a rubble-pile with $\tilde{\mu}_{rubble} = \sqrt{\tilde{\mu}/\epsilon}$, we have a linear relationship between σ_μ and μ as shown by the following equation:

$$\sigma_\mu = \frac{2}{5}\frac{\mu}{\epsilon}\sigma_{h_2}. \tag{39}$$

For this rubble-pile hypothesis, DTE Doppler measurements could be used to constrain Phobos' bulk rigidity with high precision, the latter being determined within 1%[11] after less than 40 weeks of tracking data (see Fig. 9). Note that knowledge on the bulk properties (rigidity and density) of Phobos obtained from radio science data, combined with information on the composition of the body, could lead to constraints on the proportion of rocky material and thus could answer the crucial question of the presence, or absence, of volatiles ice and/or porosity inside Phobos, and provide valuable information about the physical processes prevailing at its origin (Rosenblatt, 2011). Conversely, if Phobos is monolithic, it becomes impossible to precisely evaluate its rigidity with the observational approach considered in this study, since the precision is then proportional to μ^2 as shown in the following equation:

$$\sigma_\mu = \frac{19}{5}\left(\frac{\mu R}{\rho GM}\right)^2\sigma_{h_2}. \tag{40}$$

12. Phobos' dissipation

A precise determination of the bulk rigidity could in turn give some constraints on the global dissipation that results from the non-elasticity of the material, which is a key input to orbital evolution modeling (Lambeck, 1979). Indeed Goldreich (1963) expressed the overall tidal dissipation by separating the non-rigidity-caused and self-gravity-caused components of the tidal quality factor

$$Q = Q_0(1 + \tilde{\mu}^{-1}), \tag{41}$$

Q_0 being the value that the quality factor would have if self-gravity was absent. Given the ranges of $\tilde{\mu}$ of Table 5, one can deduce that the relative contribution from Phobos self-gravity will be smaller that 10% to the overall energy loss in response to tidal forcing even for a carbonaceous rubble-pile body. So the bulk rigidity quantity μ

[9] In fact Δr will vary a bit less than a factor of 2 (i.e., about 1.7) since h_2, inversely proportional to R, decreases of about 15% between R_0 and R_a.

[10] Note that one can deduce, from such h_2 uncertainties, precisions on k_2 Love number and $\tilde{\mu}$ simply by calculating $\sigma_{h_2} = 5/3\sigma_{k_2} = 2/5h_2^2\sigma_{\tilde{\mu}}$.

[11] Such a fine precision is a bit optimistic given the approximations made (hydrostaticity, incompressibility, sphericity) and given the fact that the uncertainties on ϵ, ρ, g and R have not been taken into account here.

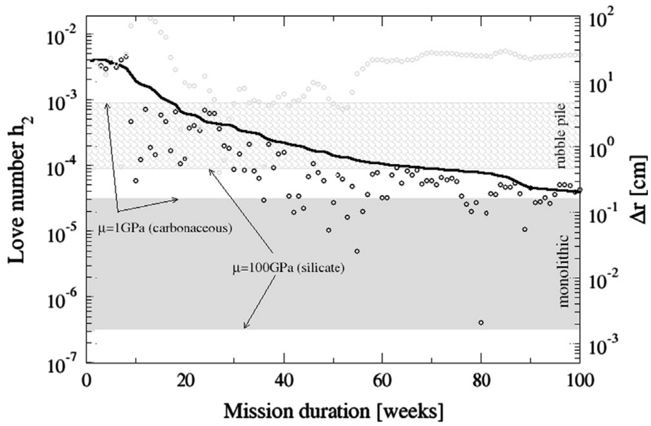

Fig. 8. Love number, h_2, and amplitude of the tidal radial displacement, Δr, as a function of the rigidity, μ, suggested for Phobos' material and for different assumptions on the moon's internal structure. Solid curve shows the evolution of the 1–σ uncertainty in h_2 (left y-axis) and the inferred uncertainty in Δr amplitude (right y-axis) as a function of the mission duration. The uniform gray area in the lower half of the plot is the range of displacement for a uniform elastic body and up-patterned area is for a rubble-pile, for a range of values for Phobos material rigidity. Black and gray dots are true errors obtained with ephemeris at centimeter and meter level of accuracy, respectively. The numerical values plotted here are obtained by considering the mean radius of Phobos: $R = 11.27$ km.

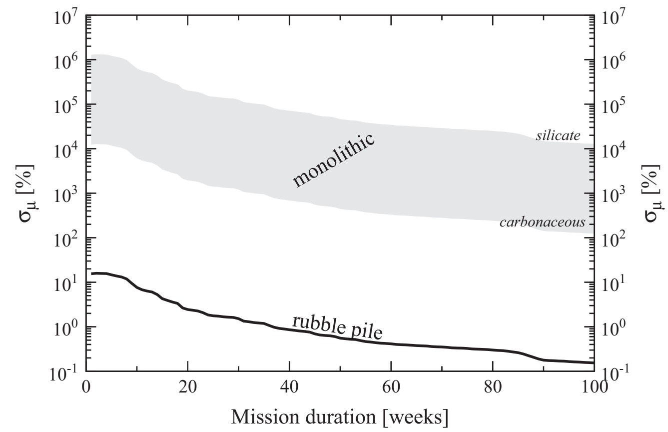

Fig. 9. Uncertainty on the rigidity, μ, in percent, as a function of mission duration. The case of a monolithic body corresponds to the uniform gray areas in the upper half of the plot. The case of a rubble-pile moon composed of irregular elements corresponds to the black solid line. The latter does not depend on the moon's composition (see text for details).

is not so much relevant in the determination of the tidal Q factor of Phobos.

Otherwise, tidal dissipation has an impact on the librations and orientation of a body. We can thus expect to estimate the overall tidal dissipation factor Q from the determination of the libration amplitudes, since the ratio of the amplitudes of the dissipative to the non-dissipative libration, p, is Rambaux et al. (2010)

$$p = 1 - \frac{k_2}{Q}\frac{3R^3n^3}{CGM}\frac{\omega_T^4}{\nu_\tau^4}\frac{(2\nu_\tau^2 - \omega_T^2)}{(\nu_\tau^2 - \omega_T^2)^2}. \tag{42}$$

However, in the case of Phobos, even by considering a huge range of plausible values for $Q \in [1, 1000]$, the small value of k_2 ($\leq 10^{-3}$, see Table 5) leads to a shift in the amplitudes of libration of Table 2 much too small ($< 10^{-16}$ degree) to be detectable.

Finally, there is a time lag between the Phobos–Mars direction and the direction of the tidal bulge raised by Mars on Phobos that depends on the mechanical properties of Phobos. This constant misalignment can be seen as a phase lag, $\Delta\varphi$, in the periodic surface displacement Δr. $\Delta\varphi$ is defined as a function of the dissipation factor through $Q^{-1} = \sin(\Delta\varphi)$ (Castillo-Rogez et al., 2011). Therefore, the precision of the Q factor can be inferred by estimating $\Delta\varphi$ and its associated error. For small lag angle, when we have $Q^{-1} \simeq \Delta\varphi$, the relative precision on Q will be similar to that on $\Delta\varphi$

$$\frac{\sigma_Q}{Q} \simeq \frac{\sigma_{\Delta\varphi}}{\Delta\varphi}. \tag{43}$$

If the expression of Δr in amplitude ($|V_t/g|h_2$) and phase ($\Delta\varphi$) is converted in sine (A^s) and cosine (A^c) amplitudes, we have precisions such that $\sigma_{A^c} \simeq \sigma_{A^s} \simeq |V_t/g|\sigma_{h_2}$. We can thus write

$$\frac{\sigma_Q}{Q} \simeq \frac{Q}{h_2}\sigma_{h_2}. \tag{44}$$

For $Q = 100$, the precision obtained after more than a Martian year is not better than about 100% even in case of a rubble-pile Phobos composed of carbonaceous material. For smaller Q the precision will be better and for values of Q greater than 100 it will be worst as clearly suggested by Eq. (44).

13. Conclusion

This analysis shows that a short geodetic mission (less than six months) is sufficient to accurately constrain Phobos' rotation, contingent upon an improvement of the ephemeris of the Martian moon achieved in the mean-time. The rotational motion of Phobos can be very precisely estimated by using star tracker and/or DTE Doppler measurements. Both data types are complementary. DTE experiment is more efficient to estimate short-period librations while ST is more suitable for the long-period librations. Therefore we point out the forcefulness of a combination of both data types with a major interest of ST data to remove Phobos ephemeris errors from the DTE measurements. The long-period libration amplitudes need a long time span of operation (between one half and one full Martian year) to be estimated at the 10^{-3} degree level of precision. Since these amplitudes are equal to the orbital variations magnitudes, one can use them as additional constraints in the computation of the Phobos' ephemeris. The short-period libration amplitudes can be estimated with a precision better than 1% in less than 20 weeks, providing strong constraints on the geophysical properties of Phobos. Indeed, the short-period libration amplitudes are direct functions of the relative difference in the moments of inertia, opening an avenue for improving our knowledge of the interior structure of this moon. It is found that the orbital period librations are the most interesting for that purpose because they lead to the best precision on $(B-A)/C$ (~10^{-5} after only 10 weeks of operation) independently from Phobos' proper frequency value. However, we have shown that inferring the main moments of inertia (MOI) with a precision better than the 10% level (current precision on these parameters) remains challenging as long as the degree-two gravity coefficients of Phobos are poorly constrained. The latter must be determined at the percent level for the MOI to be obtained with a precision sufficient to yield constraints on the potential presence of heterogeneities in the internal mass distribution of Phobos.

Assuming that Phobos' ephemeris are accurately known (at the centimeter level), it is also found that less than 70 weeks of DTE Doppler data will be needed to measure the tidal surface displacements of a rubble-pile Phobos, and this independently from the material composition. In other words, less than a Martian year of DTE operation will bring definitive constraints on the nature (rubble-pile versus monolithic) of Phobos interior, providing therefore additional constraint on its origin and evolution.

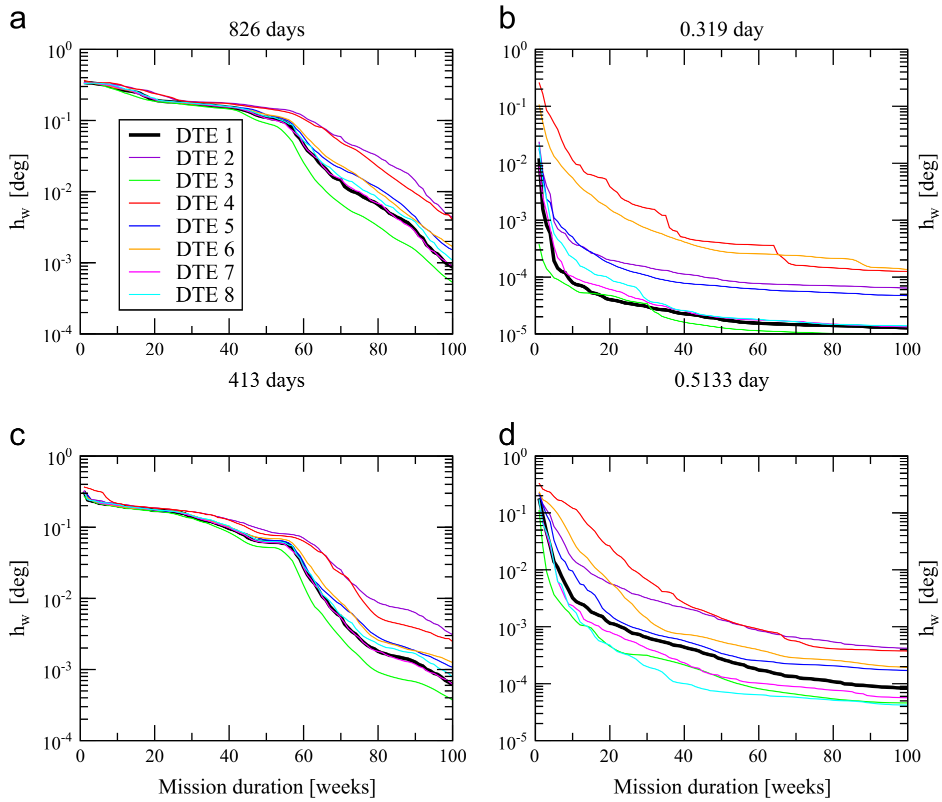

Fig. C1. Impact of Doppler operational parameters on the post-fit uncertainties of four typical amplitudes of libration in *W*. A description of each scenario is reported in Table C1. **DTE 1** is considered as baseline in this paper.

Table C1
Definition of the operational conditions tested for the Doppler experiment and plotted in Fig. C1. About 1 h of tracking correspond to 60 Doppler measurements. Boldfaced quantities refer to changes from the reference configuration (DTE 1).

Scenario	Data sampling (h)	Data noise (mm/s@60 s)	Earth elevation (deg).	Landing latitude (deg).
DTE 1	1 per day	0.05	all∈[0; 90]	+14
DTE 2	1 per day	0.25[a]	all∈[0; 90]	+14
DTE 3	1 per orbit	0.05	all∈[0; 90]	+14
DTE 4	1 per week	0.05	all∈[0; 90]	+14
DTE 5	1 per day	0.05	low∈[0; 45]	+14
DTE 6	1 per day	0.05	high∈[45; 90]	+14
DTE 7	1 per day	0.05	all∈[0; 75[b]]	**+40**
DTE 8	1 per day	0.05	all∈[0; 55[b]]	**+60**

[a] Considered as one-way data noise level in the worst case.
[b] At 40° (60°) of latitude the Earth does not appear above 75° (55°) of elevation in the lander's sky.

Table C2
Definition of the operational conditions tested for the star tracker experiment and plotted on Fig. C2.

Scenario	Data sampling pictures	Data number	Data noise (arc second)
ST 1	1 per hour	16 800	60
ST 2	1 per hour	16 800	**10**
ST 3	1 per orbit	2194	60
ST 4	1 per week	100	60
ST 5	1 per hour, 1 day per week	2400	60
ST 6	1 per day	700	60

Acknowledgments

This work was financially supported by the Belgian PRODEX program managed by the European Space Agency in collaboration with the Belgian Federal Science Policy Office. Part of this work was carried out at the Jet Propulsion Laboratory, California Institute of Technology, under Contract to NASA.

Appendix A. Lander site requirements

The landing site has to offer the best operational conditions. Considering a solar-powered lander, illumination conditions (daylight duration and Sun elevation) must enable enough power for operating over a large time span. The maximum Sun elevation, ε_s, in the sky of a lander at latitude φ can be roughly expressed as a function of φ, L_S the planetocentric longitude of the Sun and i the obliquity of Phobos (angle between its equator and the ecliptic plane which is more or less equal to Mars obliquity: $i \approx 25^\circ$) through $\varepsilon_s = \pi/2 - \varphi + i\ \sin(L_S)$. A landing site at a latitude higher than about 65° is not suitable because, due to orbital axis tilt, the Sun will remain below the local horizon during winter season preventing continuous operation during a whole Martian year.

Moreover, the higher φ, the larger the amplitude of the variation in Phobos daylight duration D_{dl} around the mean value of half the rotation period $T_{0.319}$, as it can be deduced from the following equation: $D_{dl}(\varphi) = T_{0.319} - T_{0.319}/\pi \times \arccos\ [\tan(\varphi)\ \tan(\arcsin(\sin(i)\ \sin(L_S)))]$. Once again, to maximize the illumination duration for any date of operations, it is preferable to land near the equator where the Sun is always visible 50% of the Phobos' day. For operational purposes, the landing site longitude λ appears as a less significant parameter. Indeed, since the rotation period (7.656 h) is very small with respect to the period of revolution around the Sun (687 days), ε_s and D_{dl} have little dependence on λ. However, due to the size and proximity of Mars, a lander on the near side

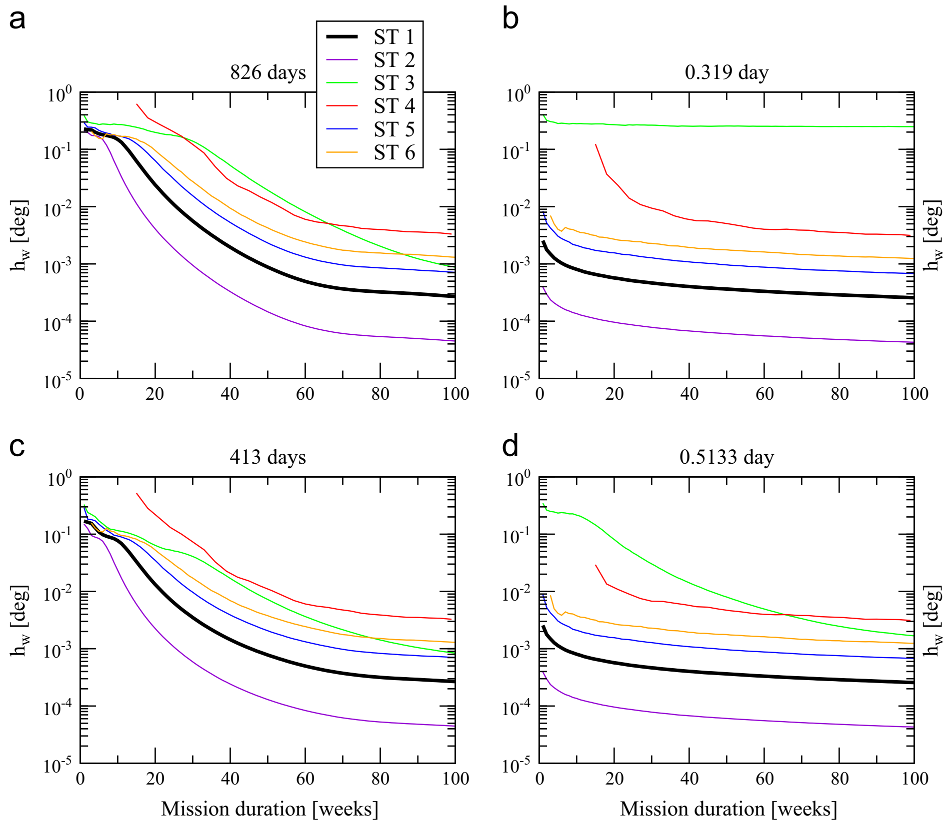

Fig. C2. Impact of star tracker operational parameters on the post-fit uncertainties of four typical amplitudes of libration in W. A description of each scenario is reported in Table C2. **ST 1** is considered as baseline in this paper.

(with $\lambda \in [-90^\circ, 90^\circ]$) would see daily solar eclipses and Earth occultations, reducing the batteries charging time (or D_{dl}) and the tracking window durations (or DTE data number) of about 20% each (corresponding to a time reduction of 50 min per orbit). In conclusion, it seems more suitable to land a probe in the far side near the equator. Note that topographic considerations have also to be taken into account.

Appendix B. Star tracker data modeling

In the following we assess the influence on the libration estimate precisions of the constant and a priori unknown rotation matrix R_κ that have been neglected in Section 3.1. If we consider that no a priori knowledge can be obtained on R_κ, the angles involved in R_κ (permitting thus to transform a vector from PBF to the ST camera reference frame) have to be estimated together with the other 38 parameters. This has major impact on the modeling of the ST observable, since α, δ and W cannot be estimated separately anymore. Therefore, the observable must be the rotation matrix M_{ST} or the associated quaternion denoted Q_{ST}. Note that, due to the compactness of the quaternion formalism (four elements against nine in the matrix form), the 1−σ uncertainties are five times smaller on average using the Q_{ST} than using the M_{ST} observable modeling, making attitude quaternions more suitable than the rotation matrix when determining libration amplitudes. However, these Q_{ST} data do not provide estimates as precise as yielded by α, δ and W separately, because of the increasing correlations among all the libration parameters with one another and with the new angles appearing in R_κ. The first approach leads to 1−σ uncertainties on average five times smaller than those obtained with the Q_{ST} data. It is noteworthy that one can also consider a by-product of the raw ST data Q_{ST}, which is the instantaneous vector of rotation, in order to solve the problem induced by R_κ. Indeed, by choosing the adequate framework (i.e., PBF), Ω, the instantaneous vector of rotation of EME2000 with respect to PBF, can be obtained by calculating $M_{ST}^{\star -1}\dot{M}_{ST}^{\star}$ (dotted quantity standing for the time derivative). Since this matrix product is equal to $M^{-1}\dot{M}$ (M being the Phobos rotation matrix, see Section 2) the new observable Ω is not a function of R_κ. However, to convert raw quaternion data into Ω data, one needs to calculate numerically $\dot{M}_{ST}^{\star}$, introducing an additional noise that leads to libration amplitude estimates several order of magnitudes less precise than those obtained in Section 4.

Appendix C. Influence of operational parameters

We investigate here the influence of some of the operational parameters (e.g., mission duration, data number and quality, etc.) on the restitution of the libration angles, in order to provide a confidence interval for the libration precisions assessed in this paper. Focused on the longitudinal[12] libration amplitudes in W, $h_W = \sqrt{W^{c^2} + W^{s^2}}$, we compare the precision that can be obtained on four different typical amplitudes depending on the data noise level and the data sampling (occurrence and coverage, i.e., the number of measurements and their repartition in time).

We consider (a) one long-period (at 826 days), large amplitude, (b) one long-period (at 413 days), small amplitude, (c) one short-period (at 0.319 day), large amplitude, (d) and one-short period (at 0.5133 day), small amplitude. Eight cases are computed for the Doppler experiment (see Fig. C1) and defined in Table C1, and six

[12] Libration amplitudes in α and δ have similar behavior.

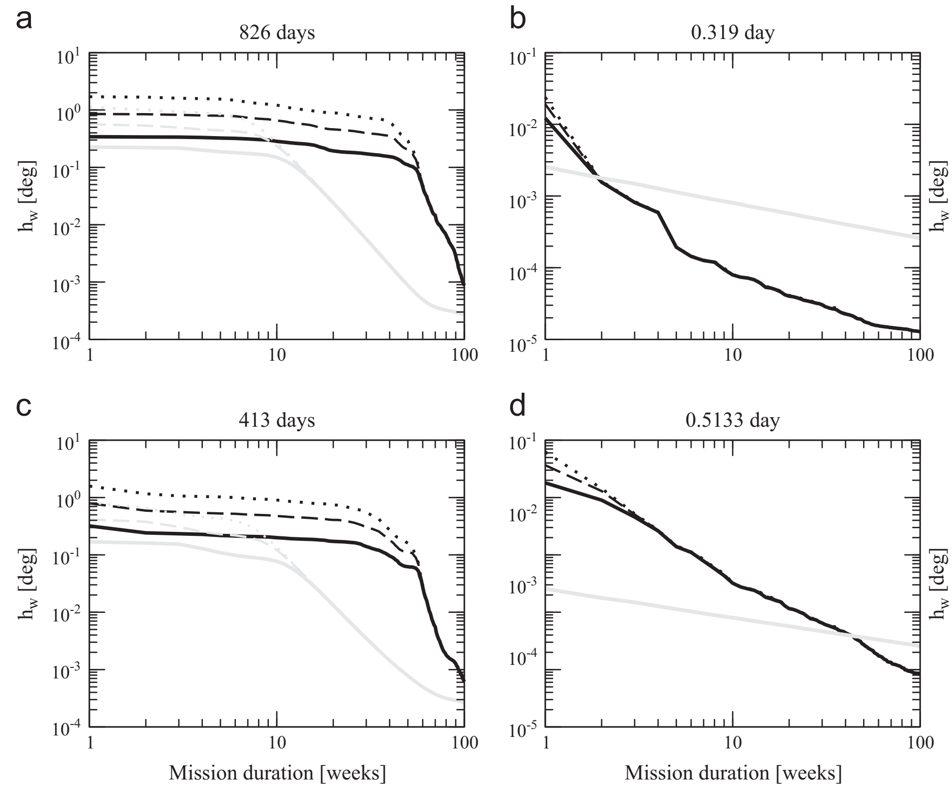

Fig. D1. Uncertainties on four typical amplitudes of the longitudinal libration in W as a function of the a priori constraint: one long-period large amplitude (at 826 days), one long-period small amplitude (at 413 days), one short-period large amplitude (at 0.319 day), and one short-period small amplitude (at 0.5133 day). Black curves are uncertainties in the Doppler solutions and gray curves correspond to star tracker solution uncertainties. Solid curves have been obtained for 0.2° of a priori constraints on all estimated librational parameters, dashed curves for 0.5°, and dotted curves for 1.0° of a priori constraints.

cases are computed for the star tracker experiment (see Table C2 and Fig. C2). Note that the 14 cases use a priori constraints of 0.2°.

The key information revealed by these various test cases is that the precision obtained in Section 4, corresponding to the black lines (DTE 1 and ST 1) in Figs. C1 and C2, has a confidence (i.e., could be in reality better or worse by) less than one order of magnitude in precision depending on the actual mission scenario and parameters for a nominal mission duration of about one terrestrial year. In more details, one can see from cases DTE 2 and ST 2 the significant effect of the data noise level shifting the 1−σ post-fit uncertainties by a factor 10 whatever the signal considered. We also see very clearly the impact of the number of data points onto the a posteriori uncertainties. Indeed, by increasing the number of data points from N^- to N^+, the a posteriori uncertainties will decrease by a factor $\sqrt{(N^- - n_p)/(N^+ - n_p)}$, where n_p is the number of estimated parameters (38 in ST and 41 in DTE). For the Doppler experiment, N^- and N^+ will not be so much different from what has been considered so far, but the ST experiment is likely to provide much more data than envisaged here, implying $N^- \ll N^+$. This means that, in particular for the ST solutions, as soon as the solutions are not driven by the a priori constraints anymore (see Section Appendix D), then the 1−σ uncertainties could be significantly smaller than those presented in Fig. C2. Nevertheless, such a large number of data points would compensate for the optimistic solutions shown in this study that are obtained assuming the constant rotation R_κ well known and α, δ and W as three distinct observables (see Section 3.1). Since the ST 3 case corresponds to an acquisition rate of one data point every 0.319 day, the post-fit precisions obtained in that particular mission scenario are poor. Indeed the precision of the libration at the orbital period remains the a priori 0.2° error, having therefore a strong negative impact on the determination of all others POP. This shows the strong limitation of a steady tracking schedule. Finally we note that the case DTE 6, corresponding to the scenario with tracking data acquired when the Earth's elevation is high in the sky of the lander, is not suitable for the short period libration determination.

Appendix D. A priori constraints influence

To stabilize the normal matrix and allow for least-square inversion, we have introduced, as is customary, a matrix of a priori constraints on estimated parameters. In this section we look at the influence of these a priori constraints on the 1−σ post-fit uncertainties. We thus consider three different a priori constraints on each estimated amplitude: 0.2°, 0.5° and 1.0°. Due to correlations, uncertainties on the DTE solutions are more strongly influenced by the a priori constraints than the ST solutions, whatever the period and amplitude of the libration signal (see Fig. D1). Star tracker solution uncertainties at short-periods depend very weakly on a priori constraints and long-period uncertainties become totally free of these constraints after about 15 weeks. This corresponds to about one-eighth of the 826-day period large amplitude and about one quarter of the 413-day period small amplitude.

The uncertainties on the DTE solutions for long-period librations depend strongly on the a priori constraints during half of the largest 826-day period (60 weeks, Fig. D1, left panels) becoming totally independent from the constraints afterwards. In the case of the short period signals, less than three weeks of Doppler tracking data are needed for the influence of the a priori constraints to vanish (see Fig. D1, right panels).

References

Andert, T.P., Rosenblatt, P., Pätzold, M., Häusler, B., Dehant, V., Tyler, G.L., Marty, J.C., 2010. Precise mass determination and the nature of Phobos. Geophysical Research Letters 37 (May), L09202, http://dx.doi.org/10.1029/2009GL041829.

Asphaug, E., Melosh, H.J., 1993. The stickney impact of Phobos: a dynamical model. Icarus 101 (1), 144–164, http://dx.doi.org/10.1006/icar.1993.1012.

Borderies, N., Yoder, C.F., 1990. Phobos' gravity field and its influence on its orbit and physical librations. Astronomy and Astrophysics 233 (July), 235–251.

Castillo-Rogez, J.C., Efroimsky, M., Lainey, V., 2011. The tidal history of Iapetus: spin dynamics in the light of a refined dissipation model. Journal of Geophysical Research Planets 116 (September), E09008, http://dx.doi.org/10.1029/2010JE003664.

Chapront-Touzé, M., 1990. Phobos' physical libration and complements to the ESAPHO theory for the orbital motion of PHOBOS. Astronomy and Astrophysics 235 (August), 447–458.

Danby, J.M.A., 1988. Fundamentals of Celestial Mechanics. Willman-Bell, Richmond.

Duxbury, T., 1989. The figure of Phobos. Icarus 78 (1), 169–180 3.

Fanale, F.P., Salvail, J.R., 1989. Loss of water from PHOBOS. Geophysical Research Letters 16 (April), 287–290, http://dx.doi.org/10.1029/GL016i004p00287.

Folkner, W.M., Planetary ephemeris DE425 for Mars Science Laboratory arrival. Jet Propulsion Laboratory—Interoffice Memorandum 343R-12-002, 2012.

Goldreich, P., 1963. On the eccentricity of satellite orbits in the solar system. Monthly Notices of the Royal Astronomical Society 126, 257.

Goldreich, P., Sari, R., 2009. Tidal Evolution of Rubble Piles. The Astrophysical Journal 691 (January), 54–60, http://dx.doi.org/10.1088/0004-637X/691/1/54.

Hurford, T.A., Greenberg, R., 2001. Tidal amplitude for a self-gravitating, compressible sphere. In: Lunar and Planetary Institute Science Conference Abstracts, Lunar and Planetary Institute, vol. 32. Technical Report, page 1741, March 2001.

Jacobson, R.A., 2010. The orbits and masses of the Martian satellites and the libration of Phobos. The Astronomical Journal 139 (February), 668–679, http://dx.doi.org/10.1088/0004-6256/139/2/668.

Konopliv, A.S., Yoder, C.F., Standish, E.M., Yuan, D.-N., Sjogren, W.L., 2006. A global solution for the Mars static and seasonal gravity, Mars orientation, Phobos and Deimos masses, and Mars ephemeris. Icarus 182 (May), 23–50, http://dx.doi.org/10.1016/j.icarus.2005.12.025.

Konopliv, A.S., Asmar, S.W., Folkner, W.M., Karatekin, Ö., Nunes, D.C., Smrekar, S.E., Yoder, C.F., Zuber, M.T., 2011. Mars high resolution gravity fields from MRO, Mars seasonal gravity, and other dynamical parameters. Icarus 211 (January), 401–428, http://dx.doi.org/10.1016/j.icarus.2010.10.004.

Korablev, O., 2009. Phobos sample return mission. In: Russian Academy of Sciences.

Lainey, V., Dehant, V., Pätzold, M., 2007. First numerical ephemerides of the Martian moons. Astronomy and Astrophysics 465 (April), 1075–1084, http://dx.doi.org/10.1051/0004-6361:20065466.

Lambeck, K., 1979. On the orbital evolution of the Martian satellites. Journal of Geophysical Research 84 (September), 5651–5658, http://dx.doi.org/10.1029/JB084iB10p05651.

Le Maistre, S., Rosenblatt, P., Rivoldini, A., Dehant, V., Marty, J.-C., Karatekin, Ö, 2012. Lander radio science experiment with a direct link between Mars and the Earth. Planetary and Space Science 68 (July (1)), 105–122, http://dx.doi.org/10.1016/j.pss.2011.12.020, ISSN 0032-0633.

Lee, P., Richards, R., Hildebrand, A., the PRIME Mission Team, 2008. The prime (Phobos reconnaissance and international Mars exploration) mission and Mars sample return. In: 39th Lunar and Planetary Institute Science Conference Abstracts, Lunar and Planetary Institute, vol. 2268. Technical Report.

Lee, P., Veverka, J., Bellerose, J., Boucher, M., Boynton, J., Braham, S., Gellert, R., Hildebrand, A., Manzella, D., Mungas, G., Oleson, S., Richards, R., Thomas, P.C., West, M.D., March 2010. Hall: a Phobos and Deimos sample return mission. In: Lunar and Planetary Institute Science Conference Abstracts, Lunar and Planetary Institute, vol. 41. Technical Report, pp. 1633.

Lee, P., Jones, T., Jaroux, B., Klupar, P.D., Bellerose, J., Chartres, J., De Rosee, R., Fong, T., Genova, A., MacCarthy, T., Mungas, G., 2011. M4: Mars moons multiple-landings mission. In: Second International Conference on the Exploration of Phobos and Deimos.

Marty, J.C., Balmino, G., Duron, J., Rosenblatt, P., Le Maistre, S., Rivoldini, A., Dehant, V., van Hoolst, T., 2009. Martian gravity field model and its time variations from MGS and Odyssey data. Planetary and Space Science 57 (March), 350–363, http://dx.doi.org/10.1016/j.pss.2009.01.004.

Michel, P., Agnolon, D., Brucato, J., Gondet, B., Korablev, O., Koschny, D., Schmitz, N., Willner, K., Zacharov, A., 2011. MMSR—a study for a Martian Moon sample return mission. In: EPSC-DPS Joint Meeting 2011, 2–7 October 2011, Nantes, France, p. 849.

Moyer, T.D., 2000. Formulation for observed and computed values of deep space network data types for navigation. Deep Space Communications and Navigation Series.

Murchie, S.L., Fraeman, A.A., Arvidson, R.E., Rivkin, A.S., Morris, R.V., 2013. Internal characteristics of Phobos and Deimos from spectral properties and density: relationship to land-forms and comparison with asteroids. LPI Contributions 1719 (March), 1604.

Oberst, J., Lainey, V., LePoncin-Lafitte, C., Dehant, V., Rosenblatt, P., Ulamec, S., Biele, J., Spurmann, J., Kahle, R., Klein, V., Schreiber, U., Schlicht, A., Rambaux, N., Laurent, P., Noyelles, B., Foulon, B., Zakharov, A., Gurvits, L., Uchaev, D., Murchie, S., Reed, C., Turyshev, S.G., Gil, J., Graziano, M., Willner, K., Wickhusen, K., Pasewaldt, A., Wählisch, M., Hoffmann, H., 2012. GETEMME—a mission to explore the Martian satellites and the fundamentals of solar system physics. Experimental Astronomy 34 (October), 243–271, http://dx.doi.org/10.1007/s10686-012-9307-0.

Petit, G., Luzum, B., et al., 2010. IERS Conventions. IERS Technical Note, 36, 1, 2010.

Rambaux, N., Castillo-Rogez, J.C., Williams, J.G., Karatekin, Ö., 2010. Librational response of Enceladus. Geophysical Research Letters 37 (February), 4202, http://dx.doi.org/10.1029/2009GL041465 4202–+.

Rambaux, N., Castillo-Rogez, J.C., Le Maistre, S., Rosenblatt, P., 2012. Rotational motion of Phobos. Astronomy and Astrophysics 548 (December), A14, http://dx.doi.org/10.1051/0004-6361/201219710.

Rosenblatt, P., 2011. The origin of the Martian moons revisited. Astronomy and Astrophysics Review 19 (August), 44, http://dx.doi.org/10.1007/s00159-011-0044-6.

Rosenblatt, P., Rivoldini, A., LeMaistre, S., Dehant, V., 2010. The internal structure and the origin of Phobos. In: First Moscow Solar System Symposium, p. 29.

Rosenblatt, P., Rivoldini, A., Rambaux, N., Dehant, V., October 2011. Mass distribution inside Phobos: a key observational constraint for the origin of Phobos. In: EPSC-DPS Joint Meeting 2011, p. 761.

Seidelmann, P.K., Abalakin, V.K., Bursa, M., Davies, M.E., deBergh, C., Lieske, J.H., Oberst, J., Simon, J.L., Standish, E.M., Stooke, P., Thomas, P.C., January 2002. Report of the IAU/IAG Working Group on Cartographic Coordinates and Rotational Elements of the Planets and Satellites: 2000. Celestial Mechanics and Dynamical Astronomy, vol. 82, pp. 83–111.

Thomas, N., Stelter, R., Ivanov, A., Bridges, N.T., Herkenhoff, K.E., McEwen, A.S., 2011. Spectral heterogeneity on Phobos and DPeimos: Hirise observations and comparisons to Mars pathfinder results. Planetary and Space Science 59 (13), 1281–1292, http://dx.doi.org/10.1016/j.pss.2010.04.018, ISSN 0032-0633.

Turyshev, Slava, Farr, William, Folkner, William, Girerd, André, Hemmati, Hamid, Murphy, Thomas, Williams, James, Degnan, John, 2010. Advancing tests of relativistic gravity via laser ranging to Phobos. Experimental Astronomy 28 (2), 209–249, http://dx.doi.org/10.1007/s10686-010-9199-9 12.

Willner, K., Oberst, J., Hussmann, H., Giese, B., Hoffmann, H., Matz, K.-D., Roatsch, T., Duxbury, T., 2010. Phobos control point network, rotation, and shape. Earth and Planetary Science Letters 294 (June), 541–546, http://dx.doi.org/10.1016/j.epsl.2009.07.033.